Alzheimer's Risk Factors Age, *APOE* Genotype, and Sex Drive Distinct Molecular Pathways

Graphical Abstract
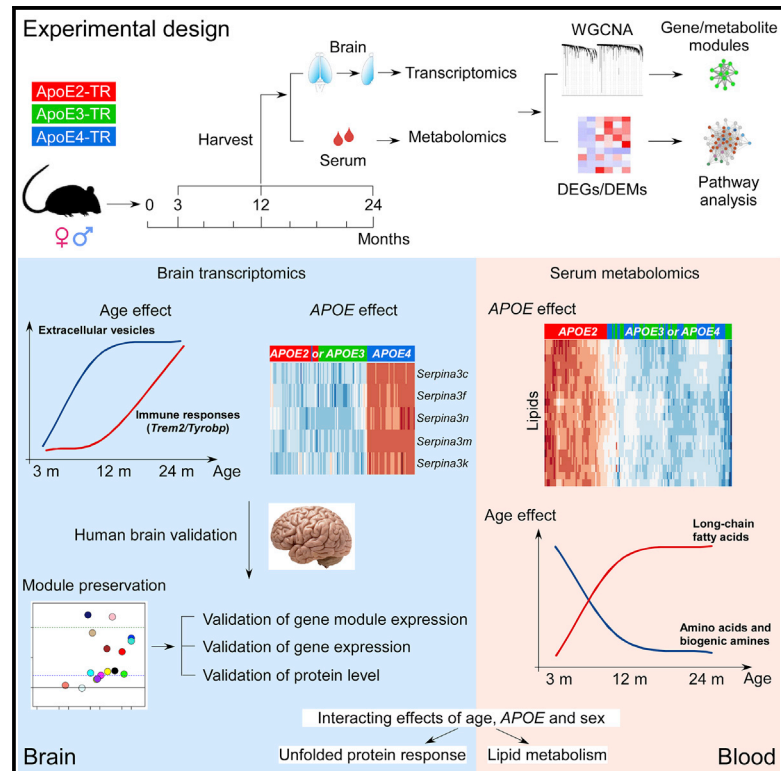
Authors

Na Zhao, Yingxue Ren,
Yu Yamazaki, ..., Takahisa Kanekiyo,
Rima Kaddurah-Daouk, Guojun Bu

Correspondence

zhao.na@mayo.edu (N.Z.),
bu.guojun@mayo.edu (G.B.)

In Brief

Zhao et al. present comprehensive datasets and analyses of brain transcriptomes and blood metabolomes from human apoE2-, apoE3-, and apoE4-targeted replacement mice across young, middle, and old ages with both sexes. The study provides critical insight on the molecular pathways underlying three major Alzheimer's risk factors age, *APOE*, and sex.

Highlights

- Aging leads to the most profound changes in brain gene expression networks

- Immune module led by Alzheimer's risk genes *Trem2/Tyrobp* is upregulated with aging

- Alzheimer's risk allele *APOE4* increases the expression of *Serpina3* family genes

- Alzheimer's protective allele *APOE2* drives unique serum metabolome profiles

CellPress

NeuroResource

Alzheimer's Risk Factors Age, *APOE* Genotype, and Sex Drive Distinct Molecular Pathways

Na Zhao,[1],[10],* Yingxue Ren,[2],[10] Yu Yamazaki,[1] Wenhui Qiao,[1] Fuyao Li,[1] Lindsey M. Felton,[1]
Siamak Mahmoudiandehkordi,[3] Alexandra Kueider-Paisley,[3] Berkiye Sonoustoun,[1] Matthias Arnold,[3],[4] Francis Shue,[5]
Jiaying Zheng,[5] Olivia N. Attrebi,[1] Yuka A. Martens,[1] Zonghua Li,[1] Ligia Bastea,[6] Axel D. Meneses,[1] Kai Chen,[1]
J. Will Thompson,[7],[8] Lisa St John-Williams,[7] Masaya Tachibana,[1] Tomonori Aikawa,[1] Hiroshi Oue,[1] Lucy Job,[1]
Akari Yamazaki,[1] Chia-Chen Liu,[1] Peter Storz,[6] Yan W. Asmann,[2] Nilüfer Ertekin-Taner,[1],[9] Takahisa Kanekiyo,[1]
Rima Kaddurah-Daouk,[3] and Guojun Bu[1],[5],[11],*

[1]Department of Neuroscience, Mayo Clinic, Jacksonville, FL 32224, USA
[2]Department of Health Sciences Research, Mayo Clinic, Jacksonville, FL 32224, USA
[3]Department of Psychiatry and Behavioral Sciences, Department of Medicine and the Duke Institute for Brain Sciences, Duke University, Durham, NC 27708, USA
[4]Institute of Bioinformatics and Systems Biology, Helmholtz Zentrum München, German Research Center for Environmental Health, Neuherberg, Bavaria 85764, Germany
[5]Neuroscience Graduate Program, Mayo Clinic, Jacksonville, FL 32224, USA
[6]Department of Cancer Biology, Mayo Clinic, Jacksonville, FL 32224, USA
[7]Duke Proteomics and Metabolomics Shared Resource, Center for Genomic and Computational Biology, Duke University, Durham, NC 27708, USA
[8]Department of Pharmacology and Cancer Biology, Duke University, Durham, NC 27701, USA
[9]Department of Neurology, Mayo Clinic, Jacksonville, FL 32224, USA
[10]These authors contributed equally
[11]Lead Contact
*Correspondence: zhao.na@mayo.edu (N.Z.), bu.guojun@mayo.edu (G.B.)
https://doi.org/10.1016/j.neuron.2020.02.034

SUMMARY

Evidence suggests interplay among the three major risk factors for Alzheimer's disease (AD): age, *APOE* genotype, and sex. Here, we present comprehensive datasets and analyses of brain transcriptomes and blood metabolomes from human apoE2-, apoE3-, and apoE4-targeted replacement mice across young, middle, and old ages with both sexes. We found that age had the greatest impact on brain transcriptomes highlighted by an immune module led by *Trem*2 and *Tyrobp*, whereas *APOE4* was associated with upregulation of multiple *Serpina3* genes. Importantly, these networks and gene expression changes were mostly conserved in human brains. Finally, we observed a significant interaction between age, *APOE* genotype, and sex on unfolded protein response pathway. In the periphery, *APOE2* drove distinct blood metabolome profile highlighted by the upregulation of lipid metabolites. Our work identifies unique and interactive molecular pathways underlying AD risk factors providing valuable resources for discovery and validation research in model systems and humans.

INTRODUCTION

Alzheimer's disease (AD) is a devastating neurodegenerative disorder characterized by the extracellular deposition of amyloid-β

(Aβ) as senile plaques and intracellular accumulation of pathological tau as neurofibrillary tangles in the brain (Blennow et al., 2006). Although the cause of sporadic AD is likely multifactorial, age is the greatest risk factor wherein 3% of people between the ages of 65 and 74, 17% of people between ages 75 and 84, and 32% of people aged 85 or older have AD (Brookmeyer et al., 1998; Hebert et al., 2013). The aging brain undergoes functional decline likely driven by decreased synaptic density and functions and is associated with inflammation induced by the reactive glial cells including astrocytes (Boisvert et al., 2018) and microglia (Kang et al., 2018; Sala Frigerio et al., 2019); however, the exact comprehension of the molecular pathways underlying the link between aging and AD is still vague. In addition to age, it is well documented that the apolipoprotein E (*APOE*) genotype (Bu, 2009; Yamazaki et al., 2019; Zhao et al., 2018a) and sex (Damoiseaux et al., 2012; Payami et al., 1994) substantially impacts the disease onset and development. The *APOE4* gene allele is the strongest genetic risk factor for late-onset AD, whereas *APOE2* is protective compared to the common *APOE3* allele (Bu, 2009; Farrer et al., 1997). Carrying one copy of *APOE4* increases the AD risk by 3- to 4-fold, and two copies by 10- to 15-fold compared to those carrying two copies of *APOE3* (Holtzman et al., 2012; Loy et al., 2014; Michaelson, 2014). Indeed, around 65% of all AD patients have at least one copy of the *APOE4* allele (Mayeux et al., 1998). Multiple Aβ-dependent and Aβ-independent mechanisms are likely involved in the risk determining effect of *APOE* polymorphism from human or mouse studies (Kanekiyo et al., 2014; Liu et al., 2017; Shinohara et al., 2016). Furthermore, epidemiological studies have demonstrated that women disproportionately suffer from dementia including AD, particularly in the elderly (Hebert et al.,

CellPress
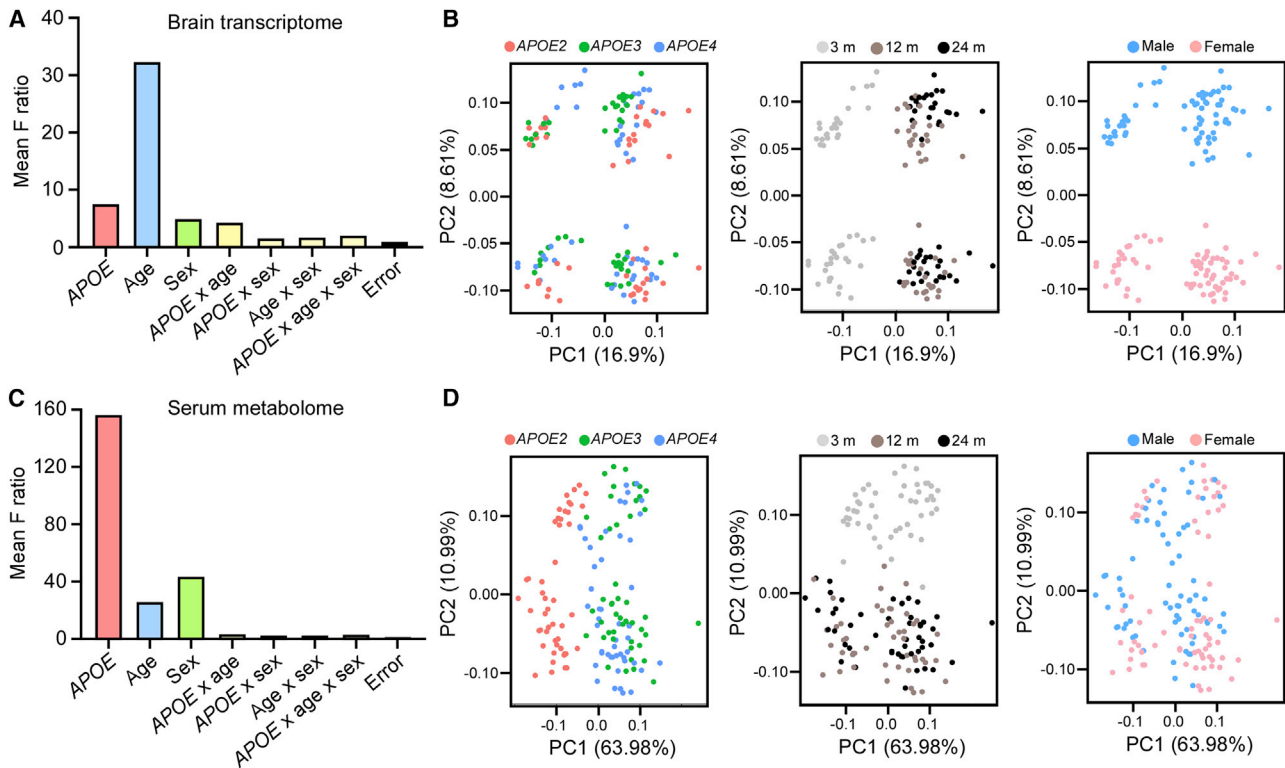
Figure 1. Global Characterization of Brain Transcriptome and Serum Metabolome Profiles of ApoE-Target Replacement Mice

(A and C) The effects of *APOE* genotype, age, sex, and their interactions on the variation of brain gene expression (A) and serum metabolite level (C) in the study cohort (n = 7–8 mice/genotype/age/sex).

(B and D) Sample-to-sample variation among brain transcriptomes (B) and serum metabolomes (D) revealed by principal-component analysis (PCA). Each circle represents a sample, colored by *APOE*, age, and sex, respectively.

2013; Mazure and Swendsen, 2016) and *APOE4* carriers (Altmann et al., 2014; Farrer et al., 1997; Neu et al., 2017). Collectively, these emerging lines of evidence suggest that age, *APOE* genotype, and sex independently and/or interactively affect the pathogenesis of AD. Investigating the molecular pathways impacted by these factors is of paramount importance to developing therapeutic strategies for AD.

Heterogeneity in humans due to genetic diversity and the impact of environmental and lifestyle differences limits the molecular study of disease mechanisms. Therefore, mouse models offer opportunities to study the effects of disease-related risk factors in a relatively pure genetic background within a controlled environment. In this study, we comprehensively profiled the brain transcriptomes and serum metabolomes of human apoE-targeted replacement (TR) mice, in which the murine *Apoe* gene locus is replaced with human *APOE2*, *APOE3*, or *APOE4* gene (Sullivan et al., 1997), at different ages and in both sexes. These apoE-TR animal models have been extensively used to assess the role of apoE isoforms in brain homeostasis and aging (Zhao et al., 2017a) or pathogenesis of amyloid (Hu et al., 2015; Tachibana et al., 2019), tau (Shi et al., 2017; Zhao et al., 2018b), and α-synuclein (Davis et al., 2020; Zhao et al., 2020). To ensure availability of our transcriptomics and metabolomics datasets for widespread utilization, we established a user-friendly web-

site (https://www.gbulab.com/searchlinks). Additionally, all datasets described in this study are available to the research community through AD Knowledge Portal (https://adknowledgeportal.synapse.org/). Guided by these datasets, we identified promising candidates of genes, metabolites, gene/metabolite co-expression networks/modules, and molecular pathways influenced by age, *APOE* genotype, and sex.

RESULTS

Profiling Strategies of Brain and Serum Samples from Mouse Models with Different *APOE* Genotype, Age, and Sex

We analyzed the cerebral cortex transcriptomics and serum metabolomics in male and female apoE2-TR, apoE3-TR and, apoE4-TR mice at 3, 12, and 24 months of age (experimental design in graphical abstract). In total, our analyses included 18 different experimental conditions (n = 7–8 mice per condition) for both transcriptomics and metabolomics. We first investigated how *APOE* genotype, age, sex, and their interactions contributed to the variation in the transcriptomics and metabolomics profiles. Interestingly, age was the strongest factor for the brain transcriptomes (Figure 1A), whereas *APOE* genotype had the greatest influence on the serum metabolomes (Figure 1C). Consistent with the source of variation analyses,
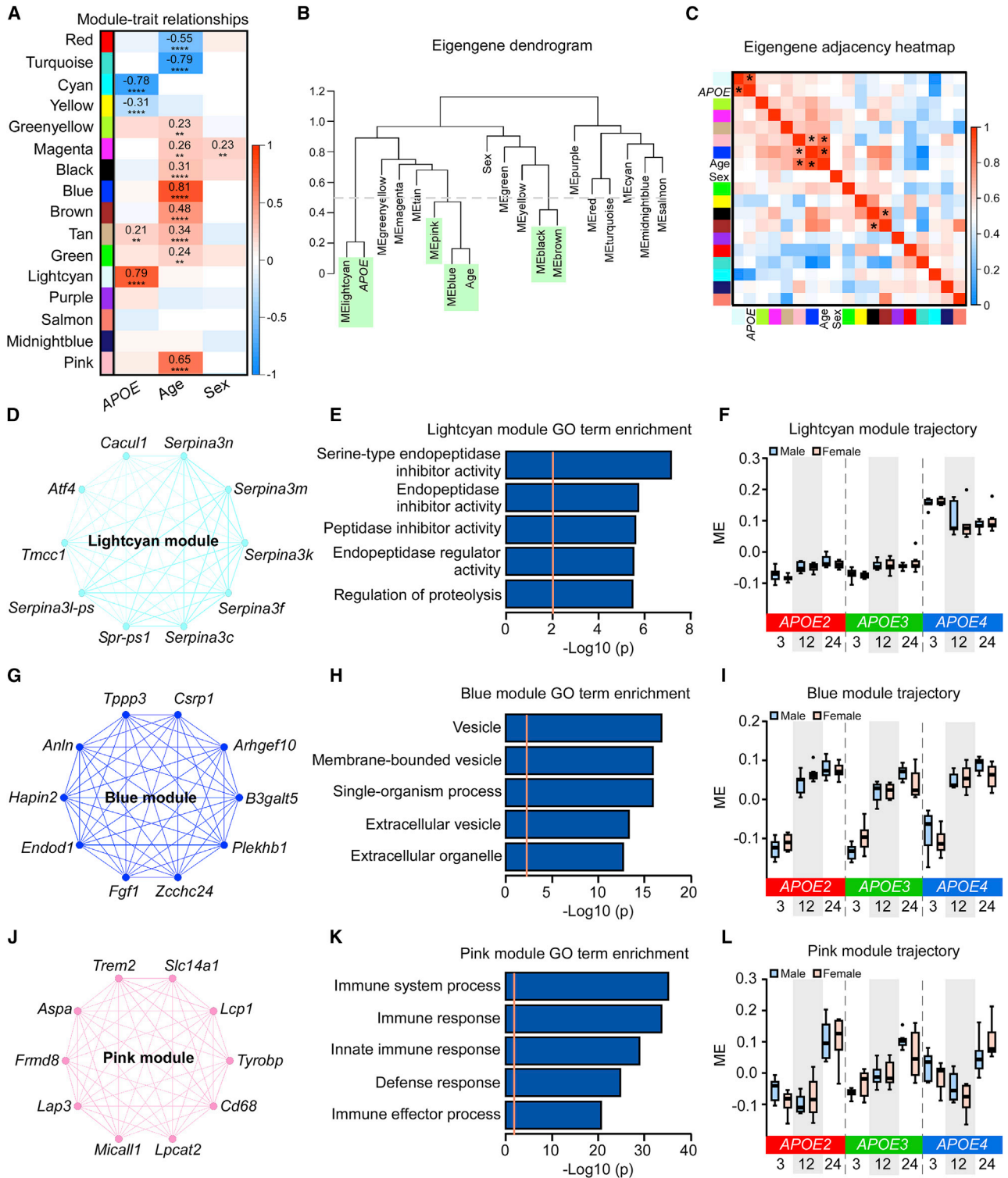
Figure 2. Impact of *APOE* Genotype, Age, and Sex on Gene Co-expression Networks of the Mouse Brain Transcriptomes

(A) The correlation between module eigengenes (MEs) and *APOE* genotype, age, and sex. The values in the heatmap are Pearson's correlation coefficients. Stars represent significant correlations: **p < 0.01; ****p < 0.0001. Modules with positive values (orange) indicate positive correlation of MEs with *APOE4* genotype, older age, or female; modules with negative values (blue) indicate negative correlation of MEs with these traits.

(B) The ME network representing the relationships between modules and between modules and *APOE* genotype, age, and sex. The y axis shows the dissimilarity of eigengenes. Modules and traits with dissimilarity score <0.5 (gray dotted line, green shadow) are considered to be tightly correlated.

(legend continued on next page)

principal-component analyses (PCAs) revealed a clear separation of the brain samples of young age cohort (3 months) from those of middle age (12 months) and old age (24 months) cohorts (Figure 1B). Although the separation between male and female was also clear by PCA, the distinguished pattern disappeared after removing the sex chromosome genes (Figure S1). Among the serum samples, a clear separation was observed between the apoE2-TR mice and other apoE-TR mice (Figure 1D).

Identification of Gene Modules Associated with *APOE* Genotype, Age, and Sex in the Mouse Brain

Next, we identified the brain transcriptional signatures affected by *APOE* genotype, age, and sex. To place gene expression changes in a systems-level framework, we performed a weighted gene co-expression network analysis (WGCNA) (Langfelder and Horvath, 2008; Zhang and Horvath, 2005) on the brain transcriptomes. We identified 16 co-expression modules (Figure 2A; Table S1). Four modules were significantly correlated with *APOE* genotype, including lightcyan, tan, cyan, and yellow (p < 0.01) (Figure 2A). Among the four modules, two were upregulated (lightcyan and tan) and two were downregulated (cyan and yellow) in *APOE4* genotype compared to *APOE2* or *APOE3* genotype (Figure 2A). Ten modules were significantly correlated with age, including eight upregulated (blue, pink, brown, tan, black, magenta, green, and greenyellow) and two downregulated modules (turquoise and red) (Figure 2A). One module, magenta, was significantly correlated with sex, and was upregulated in females compared to males (Figure 2A). Further network analysis of the eigengene and traits revealed strong correlations between the lightcyan module and *APOE* genotype; the blue, pink modules and age; and the black and brown modules (eigengene correlation of at least 0.5, Figures 2B and 2C).

To better understand the modules associated with the *APOE* genotype, we performed functional annotation of these modules and identified the top 10 intramodular hub genes in each module. The top 10 hub genes in the lightcyan module were mainly from the *Serpina3* gene family, including *Serpina3c*, *Serpina3f*, *Serpina3k*, *Serpina3l-ps*, *Serpina3m*, and *Serpina3n* (Figure 2D). Genes in this module were enriched for the regulation of endopeptidase inhibitor activity (Figure 2E). The module eigengene (ME) of the lightcyan module was upregulated in *APOE4* compared to the *APOE2* or *APOE3* genotype (Figure 2F). Additionally, the cyan module, enriched for lysosome and purine deoxyribonucleoside monophosphate metabolic processes, was significantly downregulated in the *APOE4* genotype (Figures S2A–S2C). The yellow and tan modules, enriched for RNA splicing and ribosome, respectively, were slightly upregulated in *APOE4* genotype (Figures S2D–S2F; Figures S3D–S3F).

We further examined modules associated with aging. The blue module, significantly correlated with age, was upregulated at 12 and 24 months compared to 3 months (Figure 2I). Genes in this module were enriched for processes relating to extracellular vesicles (EVs) (Figure 2H). The top hub genes in this module are known to be detected in EVs, including *Anln*, *Arhgef10*, *B3galt5*, *Csrp1*, *Endod1*, *Plekhb1*, and *Zcchc24* (Pathan et al., 2019) (Figure 2G). Furthermore, the pink module was also significantly correlated with aging, which was upregulated at 24 months compared to 3 and 12 months (Figure 2L). Genes in this module were enriched for immune response (Figure 2K), with top hub genes including *Trem2*, *Tyrobp*, and *Cd68* (Figure 2J), all of which are involved in microglial functions and immune responses in the brain (Keren-Shaul et al., 2017; Ulland and Colonna, 2018). The turquoise and red modules, enriched for respiration chain and synaptic transmission, respectively, were significantly downregulated after 12 months of age (Figures S4A–S4F). The profiles of brown, tan, black, green, greenyellow, and magenta modules slightly increased with aging and were enriched for amine biosynthetic process, ribosome, protein targeting to vacuole, intracellular membrane bounded organelle, EVs, and neurological system process, respectively (Figures S3A–S3R). The magenta module was also slightly elevated in female mice (Figures S3P–S3R).

To validate the top gene and pathway that were dysregulated by *APOE4*, we performed qPCR experiments to detect the expression of *Serpina3n*, which is the mouse ortholog of the human *SERPINA3* gene (Horvat et al., 2005). We found significantly elevated *Serpina3n* mRNA levels in *APOE4* mice at 3, 12, and 24 months of age (Figure 3A), consistent with the RNA sequencing (RNA-seq) results. The effect of *APOE4* on elevating brain Serpina3n level was further confirmed by using *in situ* hybridization to stain *Serpina3n* mRNA (Figures 3B and 3C) and western blotting to detect Serpina3n protein in an independent cohort of apoE animals (Figures 3D and 3E). To further test whether the effect of *APOE4* on regulating Serpina3n is systematic or specific to the central nervous system, we assessed the Serpina3n level in the blood, as well as in the liver where Serpina3n is synthesized and secreted into the circulation (Baker et al., 2007). Interestingly, the blood Serpina3n level was not elevated but rather decreased in *APOE4* mice compare to *APOE3* mice, and this difference was exacerbated with aging (Figure 3F), whereas the mRNA and protein levels did not differ in the liver of *APOE4* mice compared to *APOE3* mice (Figures 3G–3I). Together, these data suggest that the upregulation of Serpina3n by *APOE4* is brain specific.

Additionally, to validate the upregulated immune response with aging, we selected one of the hub genes in the pink module, *Cd68*, which encodes a lysosomal protein expressed at high

---

(C) Heatmap of the eigengene adjacency matrix. Each row and column corresponds to one eigengene (labeled by module color) or a trait of interest. Within the heatmap, orange indicates positive correlation and blue indicates negative correlation. *Correlation coefficient is above 0.5.

(D, G, and J) Network plots of the top 10 genes with the highest intramodular connectivity (hub genes) in the lightcyan (D), blue (G), and pink (J) modules.

(E, H, and K) The top 5 Gene Ontology (GO) terms enriched by 35 module genes in lightcyan module (E), 2,628 module genes in the blue module (H), and 308 module genes in the pink module (K). The orange dotted line indicates the threshold of p = 0.01.

(F, I, and L) MEs in the lightcyan (F), blue (I), and pink (L) modules across different *APOE* genotypes (*APOE2*, *APOE3*, and *APOE4*), ages (3, 12, and 24 months), and sexes (male and female). The top and bottom lines in the boxplots represent the maximum and minimum values after Tukey's test. The center line represents the median. n = 7–8 mice/genotype/age/sex.
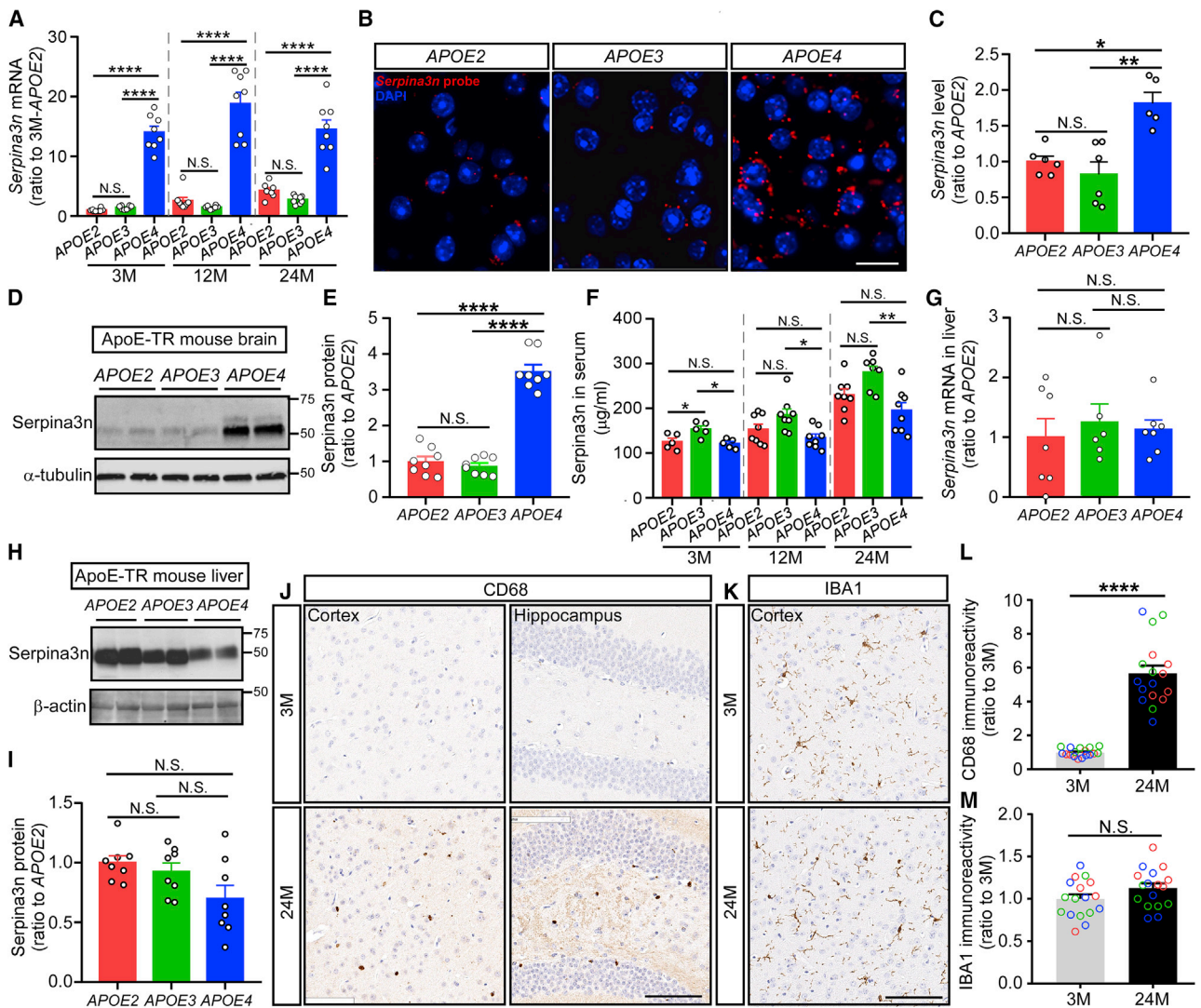
Figure 3. Validation of Serpina3n Upregulation by *APOE4* and Microglia Activation by Aging in the Brain of ApoE-TR Mice

(A) The expression of *Serpina3n* at the mRNA level was detected by qPCR using RNA samples from the cortex of apoE-TR mice at different ages (n = 7–8 mice per *APOE* genotype per age group, mixed gender). Data are expressed as mean ± SEM relative to *APOE2* mice at 3 months of age. One-way ANOVA was used to detect differences among *APOE* genotypes within each age group.

(B and C) Brain sections were prepared from the apoE-TR mice (n = 5–6 mice per *APOE* genotype, mixed gender). The expression of *Serpinas3n* was visualized using RNAscope probes while nuclei were visualized with DAPI. Representative images were shown from each *APOE* genotype, respectively (B). Scale bar: 20 μm. The intensity of *Serpina3n* staining was quantified using ImageJ software and compared among *APOE* genotypes using one-way ANOVA (C).

(D and E) Proteins from the cortex of apoE-TR mice were extracted using RIPA buffer. Serpina3n level was examined by western blotting (n = 8 mice per group, mixed gender, D). Results were normalized to α-tubulin expression. Data are expressed as mean ± SEM relative to *APOE2* mice (E). One-way ANOVA tests were used.

(F) Serpina3n in the serum of apoE-TR mice was examined by ELISA (n = 5 mice per APOE genotype at 3 months of age, n = 7–8 mice per *APOE* genotype at 12 and 24 months of age, mixed gender). One-way ANOVA tests were used to detect difference among *APOE* genotypes within each age group.

(G–I) The expression of Serpina3n at the mRNA and protein levels was evaluated in the liver of apoE-TR mice at 24 months of age by qPCR (G) or western blotting (H and I) (n = 5–6 mice per group, mixed gender, RIPA fraction was used for the western blotting experiment). The immunoblotting results were normalized to β-actin expression. Data are expressed as mean ± SEM relative to *APOE2* mice. One-way ANOVA tests were used.

(J–M) Brain sections were prepared from the apoE-TR mice at 3 and 24 months of age. Representative images are shown for the CD68 (J) and IBA1 (K) immunohistochemical staining at different brain regions. Scale bar, 100 μm. The immunoreactivity of CD68 (L) and IBA1 (M) staining in the region of cortex was evaluated by Aperio ImageScope (n = 17–18 mice per age group, mixed *APOE* genotype and gender). Red, green, and blue circles represent *APOE2*, *APOE3*, and *APOE4* genotype, respectively.

Data represent mean ± SEM relative to 3-month-old mice. Mann-Whitney *U* tests were used. *p < 0.05; **p < 0.01; ****p < 0.0001; N.S., not significant.

CellPress

levels by activated microglia and at low levels by resting microglia in the brain (Walker and Lue, 2015) and performed immunohistological staining with the brain slides from apoE-TR mice. Consistent with upregulated *Cd68* mRNA with aging, we also found significantly higher CD68 immunoreactivity in the mouse brain at 24 months of age compared to those at 3 months of age (Figure 3J and 3L), whereas the general microglia marker ionized calcium binding adaptor molecule-1 (IBA1) (Walker and Lue, 2015) did not change significantly with aging (Figures 3K and 3M), confirming the aging effects on activating microglia.

Preservation of *APOE* Genotype, Age, and Sex-Related Modules in Human AD Brains

We next assessed preservation of the *APOE* genotype, age, and sex-related modules in human post-mortem brain samples to validate their human relevance. We used the previously published RNA-seq datasets of the prefrontal cortex from Religious Orders Study and Rush Memory and Aging Project (ROSMAP) (Bennett et al., 2018) and the temporal cortex and cerebellum from the Mayo Clinic (Allen et al., 2016, 2018b). We found that 8, 10, and 9 out of 16 mouse modules were preserved in the prefrontal cortex, temporal cortex, and the cerebellum, respectively (Figures 4A, 4D, and 4G). As aging is the strongest risk factor for AD, we sought to assess whether the aging-related pink and blue mouse modules were also related to AD in humans. Interestingly, both the pink immune module and the blue EVs module were well preserved in all three human brain datasets and significantly upregulated in AD cases compared to controls in the prefrontal cortex (Figures 4B and 4C) and the temporal cortex (Figures 4E and 4F), consistent with their upregulation with aging in mouse cortex (Figures 2G–2L). In the cerebellum, the pink module did not change between AD and control (Figure 4I), but the blue module showed trending downregulation in AD cases, opposite of what we found in temporal cortex (Figure 4H). We further assessed whether the protein levels of these module genes were also affected by AD by analyzing a previously published proteomics dataset (Ping et al., 2018). Interestingly, the protein level of the pink immune module was significantly upregulated in AD cases compared to controls in the anterior cingulate gyrus and frontal cortex regions (Figure S5A), reflecting robust gene to protein association in immune response and AD in different cortical regions. However, the blue EVs module showed trending upregulation in the anterior cingulate gyrus but downregulation in frontal cortex (Figure S5B), indicating that the regulation of this module in AD might be dependent on brain regions. Taken together, our analyses show that the pink immune and blue EVs co-expression modules were conserved from mouse to human and dysregulated in AD, confirming that our findings are relevant to AD pathogenesis in humans.

The lightcyan module associated with *APOE4* was not preserved in any of the three human RNA-seq datasets (Figures 4A, 4D, and 4G). This is likely due to the fact that humans only have one *SERPINA3* protein-coding gene, whereas mice have ten protein-coding genes that are orthologous or paralogous to human *SERPINA3* (Heit et al., 2013), six of which were hub genes in the lightcyan module (Figure 2D). Consequently, we examined the expression levels of *SERPINA3* and *ATF4*, two mouse hub genes with human homologs. Interestingly, both *SERPINA3*

and *ATF4* gene expression were significantly upregulated in *APOE4* carriers compared to non-carriers in the temporal cortex (Figures 4J and 4L, left panel). Additionally, the expression of these two genes both showed upregulation in AD cases compared to controls (Figures 4K and 4M, left panel). However, the difference between *APOE4* carriers and non-carriers disappeared after adjusting for AD status (Figures 4J and 4L, right panel), whereas the upregulation was still significant in AD versus control after adjusting for *APOE4* status (Figures 4K and 4M, right panel), suggesting that the effects of AD pathology are stronger than *APOE* genotype or that the *APOE4* effects are AD dependent in these human samples.

Identification of *APOE* Genotype, Age, and Sex-Related Differentially Expressed Genes and Enriched Pathways in the Mouse Brain

We then evaluated genes with significant differential expression among different *APOE* genotypes, ages, and sexes (Table S2). We found 189 downregulated and 213 upregulated differentially expressed genes (DEGs) in *APOE2* versus *APOE3* genotypes; 117 downregulated and 144 upregulated DEGs in *APOE2* versus *APOE4* genotype, and 97 downregulated and 112 upregulated DEGs in *APOE3* versus *APOE4* genotype (Bonferroni-corrected p < 0.05, fold change ≥ 1.2). Differential expression among three *APOE* genotypes was observed in 1,813 genes (Bonferroni-corrected p < 0.05; Table S2; Figure S6A; Figures 5A–5C). Hierarchical clustering of the top 20 genes successfully separated the samples by *APOE* genotype (Figure 5D; Figures S6B, S6D, and S6F). Among these DEGs, the *Serpina3* family genes were upregulated in the *APOE4* genotype compared to *APOE2* or *APOE3* genotype, consistent with our findings from WGCNA (Figures 2D–2F). On the other hand, the expression levels of *Wdfy1*, *Alkbh6*, and *Rdh13* were lower in *APOE4* genotype. *Wdfy1* and *Alkbh6* were also hub genes in the cyan module, which was downregulated in *APOE4* (Figures S2A–S2C). Additionally, the expression levels of *Zc3h7b*, *Oscar*, *Thnsl1*, and *Tmc4* genes were downregulated in *APOE3* compared to *APOE2* or *APOE4* genotype; the *Xaf1*, *Ech1*, and *Nnt* gene expression levels were upregulated whereas the expression levels of *Olfr316*, *Lyrm7*, *Alox8*, and *Zfp14* were downregulated in *APOE2* compared to *APOE3* and *APOE4* genotype (Figure 5D). The DEGs affected by *APOE* genotypes were significantly enriched in canonical pathways such as tRNA charging, interleukin-7 (IL-7) signaling, serotonin receptor signaling, GP6 signaling, and eicosanoid signaling pathways (Figure 5E; Figures S6C, S6E, and S6G).

When comparing different ages, we identified 10,244 DEGs among three ages (Table S2). Around 3,000 DEGs were found in 12 months versus 3 months, or 24 months versus 3 months, whereas the number of DEGs between 24 months and 12 months was below 500, suggesting that the most dramatic changes of the brain transcriptomes arise between 3 and 12 months of age (Figures 5F–5H; Figure S6A). Furthermore, hierarchical clustering of the top 20 DEGs successfully separated the 3 months samples from those of the 12 and 24 months (Figure 5I; Figures S7A, S7C, and S7E). Among the top 20 DEGs, *Marcksl1*, *Gbn4*, *Snca*, and *Met* were downregulated whereas the other genes were upregulated with aging, including *Pisd*, *C4b*, *Pcdhb9*,
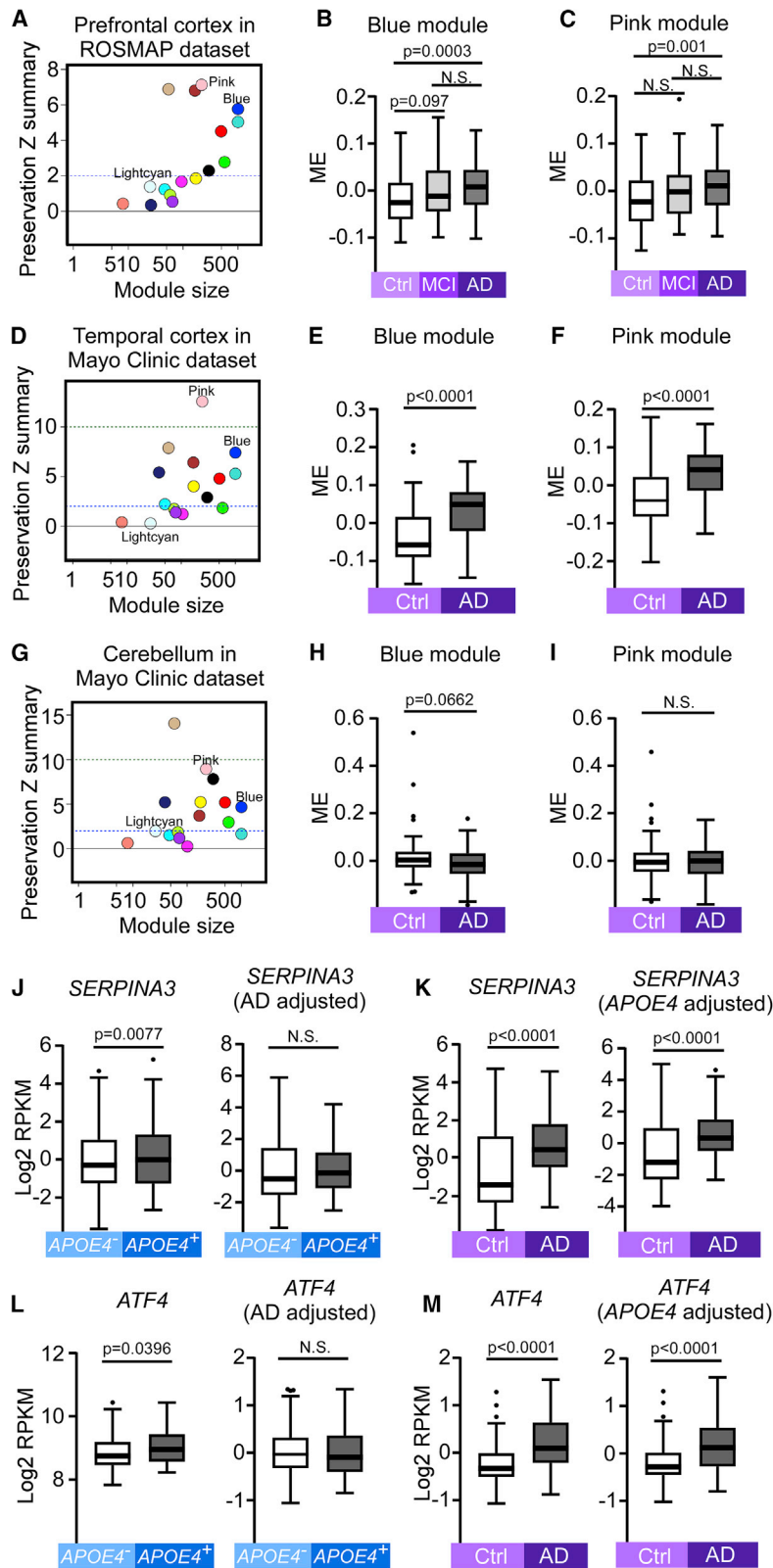
Figure 4. Module Preservation Analyses between Mouse and Human Samples

(A, D, and G) Module preservation in the ROSMAP human prefrontal cortex (A, n = 313), Mayo clinic human temporal cortex (D, n = 159), and Mayo clinic human cerebellum (G, n = 158) datasets. Preservation Z summary between 2 and 10 indicates moderate preservation. Z summary >10 indicates strong preservation.

(B and C) Blue (B) and pink (C) MEs in human control, MCI and AD samples in the ROSMAP prefrontal cortex dataset (n = 85 Ctrl, n = 78 MCI, and n = 150 AD).

(E and F) Blue (E) and pink (F) MEs in human AD and controls samples in the Mayo Clinic temporal cortex dataset (n = 77 Ctrl and n = 82 AD).

(H and I) Blue (H) and pink (I) MEs in human AD and controls samples in the Mayo Clinic cerebellum dataset (n = 76 Ctrl and n = 82 AD).

(J–M) The gene expression levels (log2 transformed reads per kilobase per million [RPKM]) of *SERPINA3* and *ATF4*, two lightcyan module genes in the Mayo Clinic human temporal cortex dataset. (J and L) The expression levels of *SERPINA3* (J) and *ATF4* (L) between *APOE4*^{-} (n = 108, including 69 Ctrl and 39 AD) and *APOE4*^{+} (n = 51, including 8 Ctrl and 43 AD) samples: left panel: expression values not adjusted by AD status; right panel: expression values adjusted by AD status.

(K and M) The expression levels of *SERPINA3* (K) and *ATF4* (M) between AD (n = 82, including 39 *APOE4*^{-} and 43 *APOE4*^{+}) and Ctrl (n = 77, including 69 *APOE4*^{-} and 8 *APOE4*^{+}) samples: left panel: expression values not adjusted by *APOE4* status; right panel: expression values not adjusted by *APOE4* status. In all boxplots, the top and bottom lines in the boxplots represent the maximum and minimum values after Tukey's test. The center line represents the median. p values were calculated by Mann-Whitney *U* tests.
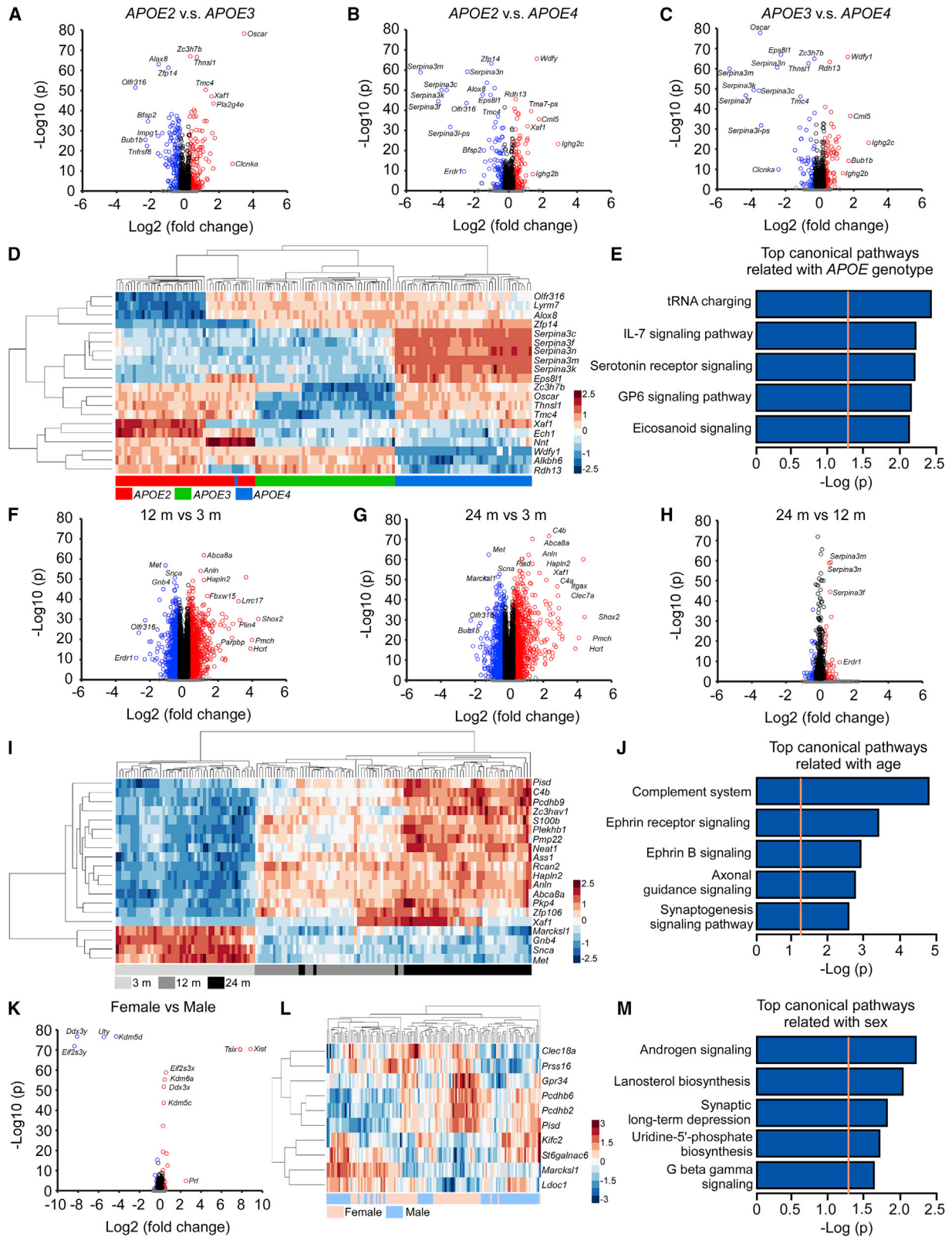
(legend on next page)

Zc3hav1, *S100b*, *Plekhb1*, *Pmp22*, *Neat1*, *Ass1*, *Rcan2*, *Hapln2*, *Anln*, *Abca8a*, *Pkp4*, *Zfp106*, and *Xaf1.* Although not in the top 20 DEG list, several *Serpina3* family genes were upregulated at 24 months compared to 12 months of age. The DEGs affected by age were significantly enriched in canonical pathways such as the complement system and ephrin receptor signaling (Figure 5J; Figures S7B, S7D, and S7F).

We next compared gene expression between sexes and identified 16 downregulated and 29 upregulated DEGs in female versus male mice (Table S2; Figure S6A; Figure 5K). The DEGs were significantly enriched in pathways such as androgen signaling, lanosterol biosynthesis, and synaptic long-term depression (Figure 5M). Hierarchical clustering of the top 10 DEGs (without genes on X or Y chromosome) did not successfully separate the samples according to sex (Figure 5L), indicating that these genes may also be regulated by other factors such as age or *APOE* genotype.

To validate the expression of these DEGs, we selected six top genes associated with either *APOE* genotype (*Serpina3n*, *Wdfy1*, and *Alkbh6*) or age (*C4b*, *Pcdhb9*, and *Plekhb1*) and performed qPCR analyses using the same samples used for RNA-seq. We found significant correlation between the values from RNA-seq and qPCR for each individual sample (Figures S8A–S8F), confirming the consistency between these two techniques. Further analysis using qPCR results showed significant dysregulation of *Serpina3n*, *Wdfy1*, and *Alkbh6* by *APOE* genotype (Figures S8G–S8I), and *C4b*, *Pcdhb9*, and *Plekhb1* by age (Figures S8J–S8L), which were all consistent with our results from RNA-seq.

Identification of Metabolite Modules Associated with *APOE* Genotype, Age, and Sex in the Mouse Serum

To assess how *APOE* genotype, age, or sex affects peripheral metabolism, we examined the serum metabolomes of our mice using the AbsoluteIDQ p180 Kit. The metabolome profiling yielded 162 metabolites after quality control (Table S3). WGCNA analysis of the metabolomes identified five co-expression metabolite modules (Figure 6A). Three modules, turquoise, yellow, and green, were significantly correlated with *APOE* genotype (Figure 6A). The MEs of all three modules were higher in *APOE2* compared to *APOE3* or *APOE4* genotype (Figures 6A, 6C, 6E, and 6G). The turquoise module contained 92 metabolites, including 65 glycerophospholipids (including phosphatidylcholine [PC] and lysophosphatidylcholine [lyso-PC]), 14 sphingolipids (including sphingomyelin and hydroxy-sphingomyelin), and 13 acylcarnitines (Table S3). The yellow module contained 11 PCs, and the green module contained 5 lyso-PCs (Table S3). Metabolites in these three modules mainly belong to lipid metabolic pathways, with an upregulation in *APOE2* compared to *APOE3* or *APOE4* genotype (Figures 6B–6G), indicating that *APOE2* drives distinct serum metabolomics signatures through the upregulation of lipid metabolism. Additionally, the yellow and green modules were also significantly correlated with sex with lower expression in females compared to males (Figures 6A and 6D–6G).

We further identified three modules that were significantly correlated with age, including two downregulated (brown and green) and one upregulated (blue) modules (Figure 6A). The brown module contained 13 amino acids and biogenic amines, and the ME was lower at 12 or 24 months of age compared to 3 months (Table S3; Figures 6H and I). The green module contained 5 lyso-PCs, which were associated with both *APOE* genotype and age (Figures 6A and F). The ME of this module was downregulated with aging in *APOE3* and *APOE4* genotype; however, this downregulation was not seen in *APOE2* genotype (Figure 6G), indicating that the protective effects of *APOE2* on aging might be linked to the preservation of lyso-PC levels. Moreover, the blue module contained 14 acylcarnitines with most of them being long-chain fatty acids, and the ME was upregulated at 12 and 24 months compared to 3 months (Figures 6J and 6K). Together, these data indicate that the effects of aging on serum metabolomics are downregulation of amino acids and biogenic amines and upregulation of acylcarnitines especially long-chain fatty acids.

Identification of *APOE* Genotype, Age, and Sex-Related Differentially Expressed Metabolites

We next studied metabolites that were significantly differentially expressed among different *APOE* genotypes, ages, and between sexes (Table S4; Figures S9A–S9D). We found 123 upregulated and 4 downregulated DEMs in *APOE2* versus *APOE3* genotype; 110 upregulated and 2 downregulated DEMs in *APOE2* versus *APOE4* genotype; 0 upregulated and 26 downregulated DEMs in *APOE3* versus *APOE4* genotype (Bonferroni-corrected $p < 0.05$, fold change ≥ 1.2); and overall 130 DEMs

---

Figure 5. Differential Gene Expression and Pathway Analyses of the Mouse Brain Transcriptomes

(A–C) Volcano plots of DEGs identified between the *APOE2* and *APOE3* (A), *APOE2* and *APOE4* (B), and *APOE3* and *APOE4* genotypes (C). The blue circles denote downregulated DEGs and the red circles denote upregulated DEGs in each comparison (Bonferroni-corrected $p < 0.05$ and fold change ≥ 1.2). The black circles denote genes with significant p values (Bonferroni-corrected $p < 0.05$) but fold change <1.2, and the gray dots denote genes that did not meet either the p value or the fold-change threshold.

(D) Hierarchical clustering of the top 20 DEGs affected by *APOE* genotypes (Bonferroni-corrected $p < 0.05$). Each row corresponds to one gene and each column corresponds to one sample.

(E) The top 5 pathways enriched by 1,011 DEGs affected by *APOE* genotypes (Bonferroni-corrected $p < 0.0001$). The orange dotted line indicates the threshold of $p = 0.05$.

(F–H) Volcano plots of DEGs identified between the 12 and 3 months (F), 24 and 3 months (G), and 24 months and 12-month-old mice (H). The color code of the circles is identical to (A)–(C).

(I) Hierarchical clustering of the top 20 DEGs affected by age (Bonferroni-corrected $p < 0.05$).

(J) The top 5 canonical pathways enriched by the top 1,000 DEGs affected by age.

(K) Volcano plot of DEGs identified between female and male mice. The color code of the circles is identical to (A)–(C).

(L) Hierarchical clustering of the top 10 DEGs affected by sex (the X- and Y-linked genes were excluded).

(M) The top 5 pathways enriched by 102 DEGs affected by sex (Bonferroni-corrected $p < 0.0001$). n = 7–8 mice/genotype/age/sex.
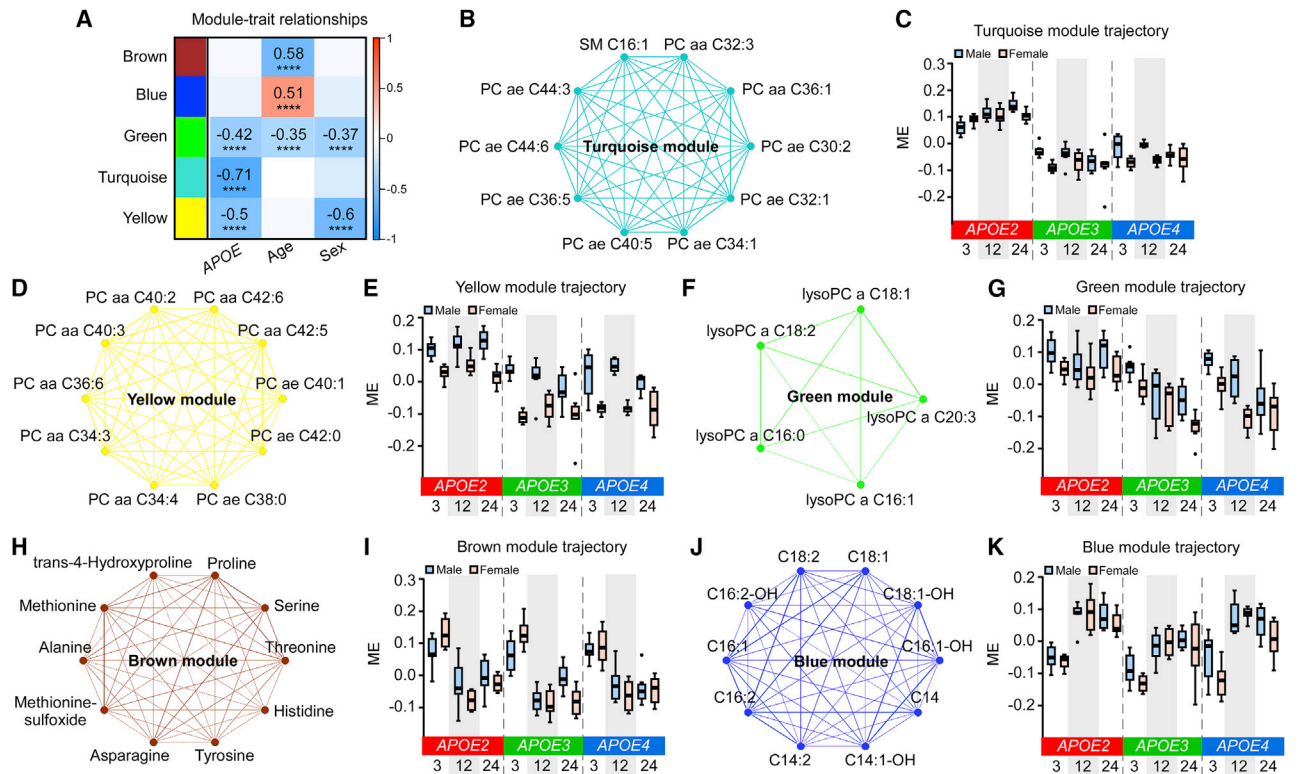
Figure 6. Impact of *APOE* Genotype, Age, and Sex on Co-expression Network of the Mouse Serum Metabolomes

(A) The correlation between MEs and *APOE* genotype, age, and sex. The values in the heatmap are Pearson's correlation coefficients. Stars represent significant correlations: ****p < 0.0001. Modules with positive values (orange) indicate positive correlation of MEs with *APOE4* genotype, older age, or female; modules with negative values (blue) indicate negative correlation of MEs with these traits.

(B, D, F, H, and J) Network plots of the top 10 hub metabolites in the turquoise (B), yellow (D), green (F, only 5 metabolites in the module), brown (H), and blue (J) modules.

(C, E, G, I, and K) MEs in the turquoise (C), yellow (E), green (G), brown (I), and blue (K) modules across different *APOE* genotypes (*APOE*2, *APOE*3, and *APOE*4), ages (3, 12, and 24 months), and sexes (male and female). The top and bottom lines in the boxplots represent the maximum and minimum values after Tukey's test. The center line represents the median. n = 7–8 mice/genotype/age/sex.

among three *APOE* genotypes (Table S4; Figure S9A; Figures 7A–7C). Hierarchical clustering of the top 20 DEMs successfully separated the samples by *APOE* genotype with *APOE2* showing distinct upregulation of lipids compared to *APOE3* and *APOE4* (Figures 7A–7C; Figure S9B), consistent with our WGCNA analysis (Figures 6B–6G).

In regard to aging, we identified 30 upregulated and 27 downregulated DEMs in 12 months versus 3 months; 30 upregulated and 31 downregulated DEMs in 24 months versus 3 months; 1 upregulated and 9 downregulated DEMs in 24 months versus 12 months of age (Table S4; Figures S9A and S9C); and overall 74 DEMs among three ages (Table S4). The small number of DEMs between 24 and 12 months indicates that the most dramatic change of serum metabolomics signatures happen in early ages, consistent with our findings in the brain transcriptomics (Figure S6A). Hierarchical clustering of the top 20 DEMs successfully separated the 3 month serum samples from that of 12 and 24 months, with downregulation of amino acids and biogenic amines and upregulation of acylcarnitines after 3 months (Figures 7D–7F), consistent with our findings from our WGCNA analysis (Figures 6H–6K).

We found 10 upregulated and 68 downregulated DEMs in female versus male mice (Table S4; Figure S9A and S9D). The top 20 DEMs were all lipids, but the hierarchical clustering of these DEMs did not clearly separate sexes (Figures 7G–7I), indicating that the effects of sex on lipid metabolism might be strongly influenced by other factors such as *APOE* genotype.

Interactions of *APOE* Genotype, Age, and Sex on Brain Transcriptomes and Serum Metabolomes

We finally assessed how the three AD risk factors, *APOE* genotype, age, and sex, interactively affect the brain transcriptomes and serum metabolomes. We identified 776 brain DEGs (Bonferroni-corrected p < 0.0001) affected by the interactions of *APOE* genotype, age, and sex. These genes were enriched in canonical pathways such as unfolded protein response, autophagy, tight junction signaling, and endoplasmic reticulum stress pathway (Figure S10B), all of which are closely related to neurodegenerative disorders such as AD (Gerakis and Hetz, 2018; Scheper and Hoozemans, 2015; Uddin et al., 2018; Yamazaki and Kanekiyo, 2017). Hierarchical clustering of the top 20 DEGs showed strong interacting effects of age and *APOE* genotype (Figure S10A).
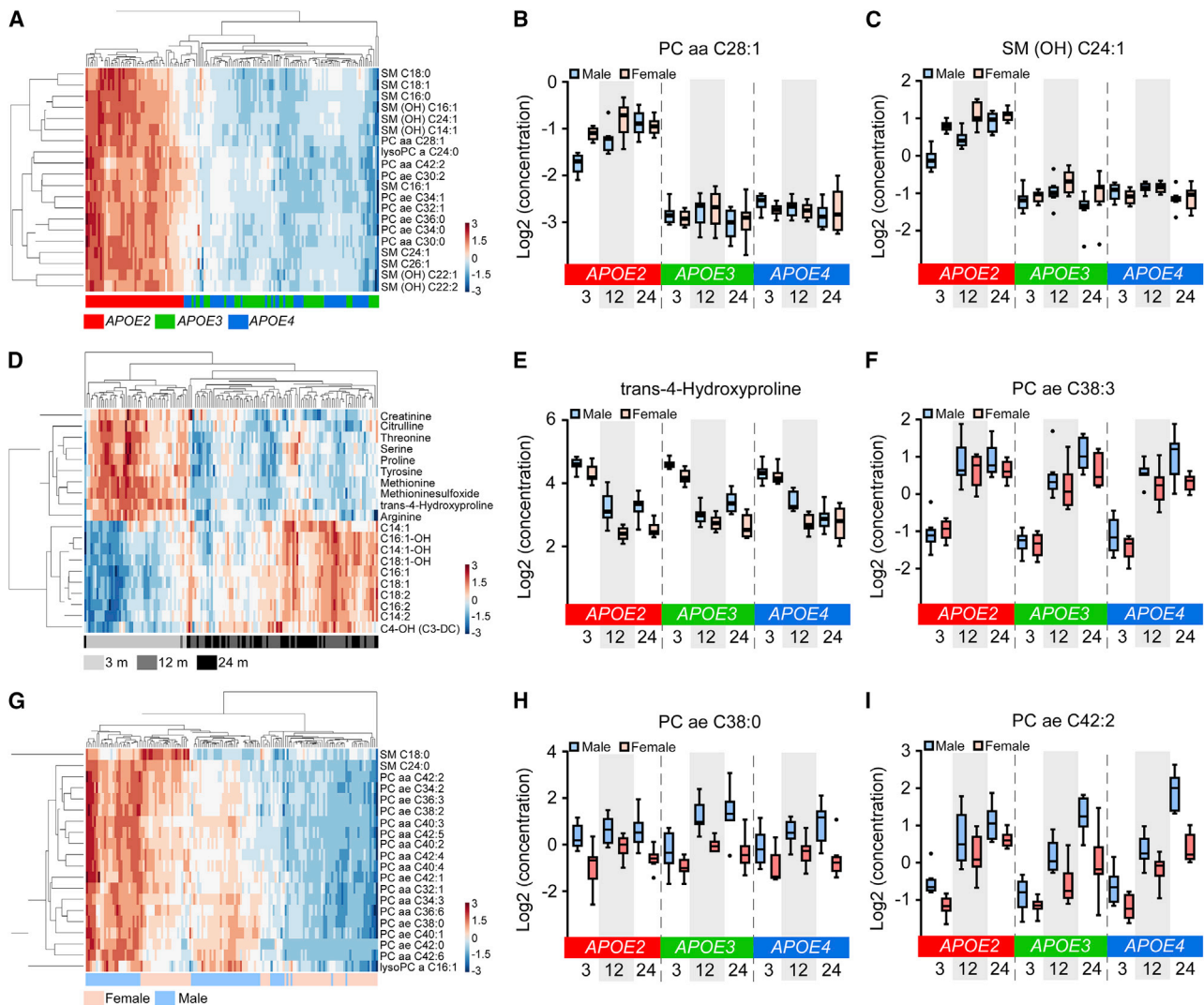
Figure 7. Differentially Expressed Metabolites in the Mouse Serum

(A, D, and G) Hierarchical clustering of the top 20 DEMs affected by *APOE* genotypes (A), age (D), or sex (G) (Bonferroni-corrected p < 0.05).

(B, C, E, F, H, and I) The expression levels of the top 2 DEMs in the comparison among *APOE* genotypes (B and C), ages (E and F), or sexes (H and I). The top and bottom lines in the boxplots represent the maximum and minimum values after Tukey's test. The center line represents the median. n = 7–8 mice/genotype/age/sex.

In particular, *APOE4* was distinct from *APOE2* and *APOE3* at 3 months, whereas *APOE2* at 12 and 24 months showed distinct signature from the other groups (Figure S10A). Interestingly, all age groups from *APOE3* genotype clustered together, indicating that the influence of aging on *APOE3* genotype was minimal. These data suggest that the effects of age on brain transcriptomic profiles were influenced by *APOE* genotype. The sex effect was not dominant under any age or *APOE* genotype group.

We further identified 68 serum DEMs synergistically affected by *APOE* genotype, age, and sex (Bonferroni-corrected p < 0.05) (Table S4, Figure S10C). Hierarchical clustering of these DEMs showed distinct separation of *APOE2* from *APOE3* and *APOE4* with significant upregulation of lipids (Figure S10C), consistent with our PCA, WGCNA and DEM analyses (Figure 1D; Figures 6B–6G; Figures 7A–7C). The effects of age and sex on

serum metabolites were observed within *APOE2* genotype but were less apparent in *APOE3* and *APOE4* (Figure S10C), further indicating that the *APOE2* genotype is the main driver for the distinct serum metabolomics profiles in our mouse cohort.

DISCUSSION

Numerous genetic and functional studies have indicated the individual and interactive effects of age, *APOE* genotype, and sex on AD risk; however, the underlying molecular pathways remained elusive. By taking the triad of AD risk factors into consideration in animal models, we investigated the molecular signatures of transcriptomics in the brain and metabolomics in the blood using apoE-TR mice at young, middle, and old ages in both sexes. Rather than focusing on *a priori* candidate genes

CellPress

or metabolites, we pursued an unbiased systems-based approach using multiple types of bioinformatics analyses to identify gene and metabolite networks and molecular pathways. Importantly, our study demonstrated that the major age- or *APOE* genotype-related genes, gene modules, and pathways identified in the mouse cortex were also significantly dysregulated in human AD temporal cortex, further supporting the profound relationship and overlap between increasing age and AD (Xia et al., 2018). We also considered the principles of regional vulnerability and disease trajectories (Fu et al., 2018) and found that the major gene networks associated with aging in animal models were altered in brain areas that show signs of pathology such as the temporal cortex, but not in the cerebellum, a brain region that is for the most part spared in AD (Allen et al., 2018a; Conway et al., 2018). The validation of gene modules at the protein level also suggests that the dysregulation of these co-expressed gene networks in AD might be brain region dependent.

We identified two major age-related gene modules in the mouse cortex, including the immune and EVs modules, which were well preserved in human brains and upregulated in the temporal cortex of AD cases compared to control subjects. While aging was the greatest contributor to the brain transcriptomics signature in our mouse models, a gene module of "immune response" was significantly upregulated at 24 months compared to 12 and 3 months of age. This module was led by the top hub genes including *Trem2* and *Tyrobp*. Although the R47H risk variant of the *TREM2* gene has been defined as a genetic risk factor of AD (Guerreiro et al., 2013; Jonsson et al., 2013), and the triggering receptor expressed on myeloid cells 2/TYRO Protein Tyrosine Kinase Binding Protein (TREM2/TYROBP) signaling are well known as regulators of microglial functions in the brain (Deczkowska et al., 2018; Poliani et al., 2015; Rangaraju et al., 2018; Song and Colonna, 2018), our study is the first to capture the aging-mediated dysregulation of *Trem2/Tyrobp* and their gene network (308 genes) using a unbiased systems-based approach in animal models. Further validation of this gene module in human brains, especially the upregulation in several cortical brain regions of AD cases compared to controls from both gene expression levels and protein levels, indicates the common changes between aging and AD regarding immune responses led by TREM2/TYROBP signaling (Zhang et al., 2013), although the validation using human aging brains without AD is necessary when the datasets become available. In addition, since the dysregulation of "EVs" module was predominantly affected in aged mouse brains or in human AD brains, our results imply the roles of EVs in maintaining CNS homeostasis and contributing to neurodegenerative disease pathology including AD. Dynamic brain functions rely upon communication among different cell types, and EVs have emerged as key mediators of such communication (Delpech et al., 2019). All cell types in the brain could release EVs, which can either be taken up by neighboring cells or released into the cerebrospinal fluid and blood (Colombo et al., 2014). Thus, they display a harmonious beneficial and detrimental role in response to CNS injury, mediating inflammatory response and inflammation-related neuroprotection, spreading senescence, as well as propagating pathogenic proteins such as Aβ, α-synuclein, and tau (Basso and Bonetto,

2016; Coleman and Hill, 2015; Delpech et al., 2019; Effenberger et al., 2014). Therefore, comprehensive investigation focusing on the biology of EVs, including the biogenesis, release, action, and the profiles of isolated EVs, will be extremely valuable.

Interestingly, age, *APOE* genotype, and sex interactively impacted pathways led by unfolded protein response (UPR) in the brain. The UPR pathway is activated to protect cells under ER stress when the inability of cells to properly fold, modify, and assemble secretory and transmembrane proteins leads to the accumulation of misfolded proteins in the ER (Walter and Ron, 2011). However, the maladaptive UPR signaling under chronic ER stress alternatively commits cells to degeneration, which is implicated in the etiology and pathogenesis of various neurodegenerative disorders including AD (Pitale et al., 2017; Scheper and Hoozemans, 2015). Our study suggests that the signaling components of the UPR might be potential targets for intervention and treatment of AD (Maly and Papa, 2014).

Furthermore, to our knowledge, our study is the first to report the correlation of *APOE* genotype and *Serpina3n/SERPINA3* gene expression in both mouse and human brains. *Serpina3n/ SERPINA3* gene encodes α1-antichymotrypsin (ACT), which is an acute phase serum glycoprotein belonging to a class of serine protease inhibitors (Padmanabhan et al., 2006). ACT inhibits the activity of chymotrypsin and cathepsin G, thus playing an important role in inflammation, complement activation, and apoptosis (Irving et al., 2000; Law et al., 2006). It has also been broadly reported that ACT is elevated in AD brains, and may promote Aβ polymerization and amyloid formation (Abraham et al., 1988, 1990, 2000; McGeer et al., 1990; Pasternack et al., 1989), consistent with our findings from the human brain datasets. In the brain, it was reported that *Serpina3n* gene is expressed by astrocytes and has recently been identified as a strong marker for reactive and aged astrocytes in the mouse brain (Boisvert et al., 2018; Zamanian et al., 2012). Interestingly, the oligodendroglia in the experimental autoimmune encephalomyelitis mouse model displayed elevated *Serpina3n* expression (Falcão et al., 2018). Notably, our study suggests an important role of apoE4 in the regulation of Serpina3n expression in the brain, although the underlying mechanisms remain unclear on how apoE4 elevates the expression of Serpina3n, which cell types are involved, and what the functional impacts linked to the elevated Serpina3n in apoE4 mice are. The upregulation of *Serpina3n* in *APOE4* genotype might be related with the pathogenic effect of apoE4 on astrocyte activation and might thus contribute to the role of apoE4 in AD pathogenesis (Fernandez et al., 2019; Perez-Nievas and Serrano-Pozo, 2018; Zhu et al., 2012). Additionally, the *Serpina3n* gene expression was upregulated at 24 months compared to 12 months of age, suggesting the common effects of *APOE4* and aging on astrocyte activation in the brain (Boisvert et al., 2018; Zamanian et al., 2012). Interestingly, in periphery such as liver and blood, the level of Serpina3n was not elevated in *APOE4* mice, indicating the upregulation of *APOE4* on Serpina3n expression is brain specific. Therefore, a better understanding of the regulation of *Serpina3n* by *APOE4* and aging in both the central nervous and periphery systems is needed such that potential biomarkers, tractable pathways, and drug targets can be defined for early diagnosis or to reduce *APOE4*- and aging-related AD risk.

CellPress

ApoE lipoprotein particles in circulation play a critical role in regulating the peripheral lipid metabolism. Although it has been reported that apoE isoforms differentially impact peripheral lipid metabolism in humans (Karjalainen et al., 2019; Phillips, 2014), our study is the first to examine the *APOE* genotype effect on blood metabolomics in a well-defined animal cohort. We found distinct serum metabolite profiles in *APOE2* mice with dramatically upregulated lipid levels (including phospholipids and sphingolipids) compared to *APOE3* and *APOE4* mice, likely due to its reduced binding affinity to apoE receptors including the LDL receptor, which might consequently elevate apoE levels and lipids in the blood (Kowal et al., 1990; Mahley, 2016; Rasmussen et al., 2015; Schneider et al., 1981). This dramatic effect of *APOE2* on lipid levels is consistent with a recently published human study (Karjalainen et al., 2019). Interestingly, lower levels of blood phospholipids are related to the phenoconversion from normal to either amnestic mild cognitive impairment or AD (Mapstone et al., 2014), suggesting that the protective effects of *APOE2* on AD risk might be associated with the elevated phospholipid profiles. However, the role of *APOE2* has been debated on one hand to be protective against AD but on the other hand to promote vascular disease (Lahoz et al., 2001; Wilson et al., 1994) and the risk for type III hyperlipoproteinemia (Kowal et al., 1990; Schneider et al., 1981) when combined with additional genetic or environmental stress, e.g., obesity, high-fat diet, and different races (Phillips, 2014; Zhao et al., 2017b). Further studies on apoE isoform-specific effects on lipid metabolism and related pathways offer great promise for a more comprehensive understanding of *APOE* genotype effects on AD to establish mechanism-based therapy. While the effect of sex on serum metabolomics is not prominent in our study, it is possible that the dominant effects of age and *APOE* genotype masked the sex effects.

In conclusion, our comprehensive data support unique and interactive molecular pathways underlying the three major risk factors for AD and map the landscape regarding how they collectively drive AD risk. These resources provide therapeutic insights into treating AD and will facilitate discovery and validation research in model systems and humans.

STAR★METHODS

Detailed methods are provided in the online version of this paper and include the following:

- KEY RESOURCES TABLE
- LEAD CONTACT AND MATERIALS AVAILABILITY
- EXPERIMENTAL MODEL AND SUBJECT DETAILS
  - ○ Mice
  - ○ Humans
- METHOD DETAILS
  - ○ Brain tissue RNA extraction, library preparation and sequencing
  - ○ Serum metabolites detection
  - ○ Mouse tissue preparation for validation experiments
  - ○ Histology and immunohistochemistry
  - ○ *In situ* hybridization
  - ○ Western blotting

  - ○ Serpina3 ELISA
  - ○ qPCR analysis
- QUANTIFICATION AND STATISTICAL ANALYSIS
  - ○ RNA and metabolites quantification, quality control and normalization
  - ○ Differential gene expression, hierarchical clustering and pathway analysis
  - ○ Weighted gene co-expression network analysis of the mouse transcriptomes
  - ○ Module preservation analysis in human RNA samples
  - ○ Module validation in human proteomics samples
  - ○ Differential metabolite expression analysis
  - ○ Metabolite co-expression network analysis
  - ○ Statistical analyses for validation experiments
- DATA AND CODE AVAILABILITY
- ADDITIONAL RESOURCES

CellPress

REFERENCES

Abraham, C.R., Selkoe, D.J., and Potter, H. (1988). Immunochemical identification of the serine protease inhibitor alpha 1-antichymotrypsin in the brain amyloid deposits of Alzheimer's disease. Cell *52*, 487–501.

Abraham, C.R., Shirahama, T., and Potter, H. (1990). Alpha 1-antichymotrypsin is associated solely with amyloid deposits containing the beta-protein. Amyloid and cell localization of alpha 1-antichymotrypsin. Neurobiol. Aging *11*, 123–129.

Abraham, C.R., McGraw, W.T., Slot, F., and Yamin, R. (2000). Alpha 1-antichymotrypsin inhibits A beta degradation in vitro and in vivo. Ann. N Y Acad. Sci. *920*, 245–248.

Allen, M., Carrasquillo, M.M., Funk, C., Heavner, B.D., Zou, F., Younkin, C.S., Burgess, J.D., Chai, H.S., Crook, J., Eddy, J.A., et al. (2016). Human whole genome genotype and transcriptome data for Alzheimer's and other neurodegenerative diseases. Sci. Data *3*, 160089.

Allen, M., Wang, X., Burgess, J.D., Watzlawik, J., Serie, D.J., Younkin, C.S., Nguyen, T., Malphrus, K.G., Lincoln, S., Carrasquillo, M.M., et al. (2018a). Conserved brain myelination networks are altered in Alzheimer's and other neurodegenerative diseases. Alzheimers Dement. *14*, 352–366.

Allen, M., Wang, X., Serie, D.J., Strickland, S.L., Burgess, J.D., Koga, S., Younkin, C.S., Nguyen, T.T., Malphrus, K.G., Lincoln, S.J., et al. (2018b). Divergent brain gene expression patterns associate with distinct cell-specific tau neuropathology traits in progressive supranuclear palsy. Acta Neuropathol. *136*, 709–727.

Altmann, A., Tian, L., Henderson, V.W., and Greicius, M.D.; Alzheimer's Disease Neuroimaging Initiative Investigators (2014). Sex modifies the APOE-related risk of developing Alzheimer disease. Ann. Neurol. *75*, 563–573.

Baker, C., Belbin, O., Kalsheker, N., and Morgan, K. (2007). SERPINA3 (aka alpha-1-antichymotrypsin). Front. Biosci. *12*, 2821–2835.

Basso, M., and Bonetto, V. (2016). Extracellular Vesicles and a Novel Form of Communication in the Brain. Front. Neurosci. *10*, 127.

Bennett, D.A., Buchman, A.S., Boyle, P.A., Barnes, L.L., Wilson, R.S., and Schneider, J.A. (2018). Religious Orders Study and Rush Memory and Aging Project. J. Alzheimers Dis. *64* (s1), S161–S189.

Blennow, K., de Leon, M.J., and Zetterberg, H. (2006). Alzheimer's disease. Lancet *368*, 387–403.

Boisvert, M.M., Erikson, G.A., Shokhirev, M.N., and Allen, N.J. (2018). The Aging Astrocyte Transcriptome from Multiple Regions of the Mouse Brain. Cell Rep. *22*, 269–285.

Brookmeyer, R., Gray, S., and Kawas, C. (1998). Projections of Alzheimer's disease in the United States and the public health impact of delaying disease onset. Am. J. Public Health *88*, 1337–1342.

Bu, G. (2009). Apolipoprotein E and its receptors in Alzheimer's disease: pathways, pathogenesis and therapy. Nat. Rev. Neurosci. *10*, 333–344.

Coleman, B.M., and Hill, A.F. (2015). Extracellular vesicles–Their role in the packaging and spread of misfolded proteins associated with neurodegenerative diseases. Semin. Cell Dev. Biol. *40*, 89–96.

Colombo, M., Raposo, G., and Théry, C. (2014). Biogenesis, secretion, and intercellular interactions of exosomes and other extracellular vesicles. Annu. Rev. Cell Dev. Biol. *30*, 255–289.

Conway, O.J., Carrasquillo, M.M., Wang, X., Bredenberg, J.M., Reddy, J.S., Strickland, S.L., Younkin, C.S., Burgess, J.D., Allen, M., Lincoln, S.J., et al. (2018). ABI3 and PLCG2 missense variants as risk factors for neurodegenerative diseases in Caucasians and African Americans. Mol. Neurodegener. *13*, 53.

Damoiseaux, J.S., Seeley, W.W., Zhou, J., Shirer, W.R., Coppola, G., Karydas, A., Rosen, H.J., Miller, B.L., Kramer, J.H., and Greicius, M.D.; Alzheimer's Disease Neuroimaging Initiative (2012). Gender modulates the APOE ε4 effect in healthy older adults: convergent evidence from functional brain connectivity and spinal fluid tau levels. J. Neurosci. *32*, 8254–8262.

Davis, A.A., Inman, C.E., Wargel, Z.M., Dube, U., Freeberg, B.M., Galluppi, A., Haines, J.N., Dhavale, D.D., Miller, R., Choudhury, F.A., et al. (2020). *APOE* genotype regulates pathology and disease progression in synucleinopathy. Sci. Transl. Med. *12*. Published online February 5, 2020. https://doi.org/10.1126/scitranslmed.aay3069.

Deczkowska, A., Keren-Shaul, H., Weiner, A., Colonna, M., Schwartz, M., and Amit, I. (2018). Disease-associated microglia: a universal immune sensor of neurodegeneration. Cell *173*, 1073–1081.

Delpech, J.C., Herron, S., Botros, M.B., and Ikezu, T. (2019). Neuroimmune Crosstalk through Extracellular Vesicles in Health and Disease. Trends Neurosci. *42*, 361–372.

Effenberger, T., von der Heyde, J., Bartsch, K., Garbers, C., Schulze-Osthoff, K., Chalaris, A., Murphy, G., Rose-John, S., and Rabe, B. (2014). Senescence-associated release of transmembrane proteins involves proteolytic processing by ADAM17 and microvesicle shedding. FASEB J. *28*, 4847–4856.

Falcão, A.M., van Bruggen, D., Marques, S., Meijer, M., Jäkel, S., Agirre, E., Samudyata, Floriddia, E.M., Vanichkina, D.P., Ffrench-Constant, C., et al. (2018). Disease-specific oligodendrocyte lineage cells arise in multiple sclerosis. Nat. Med. *24*, 1837–1844.

Farrer, L.A., Cupples, L.A., Haines, J.L., Hyman, B., Kukull, W.A., Mayeux, R., Myers, R.H., Pericak-Vance, M.A., Risch, N., and van Duijn, C.M.; APOE and Alzheimer Disease Meta Analysis Consortium (1997). Effects of age, sex, and ethnicity on the association between apolipoprotein E genotype and Alzheimer disease. A meta-analysis. JAMA *278*, 1349–1356.

Fernandez, C.G., Hamby, M.E., McReynolds, M.L., and Ray, W.J. (2019). The Role of APOE4 in Disrupting the Homeostatic Functions of Astrocytes and Microglia in Aging and Alzheimer's Disease. Front. Aging Neurosci. *11*, 14.

Fu, H., Hardy, J., and Duff, K.E. (2018). Selective vulnerability in neurodegenerative diseases. Nat. Neurosci. *21*, 1350–1358.

Gerakis, Y., and Hetz, C. (2018). Emerging roles of ER stress in the etiology and pathogenesis of Alzheimer's disease. FEBS J. *285*, 995–1011.

Guerreiro, R., Wojtas, A., Bras, J., Carrasquillo, M., Rogaeva, E., Majounie, E., Cruchaga, C., Sassi, C., Kauwe, J.S., Younkin, S., et al.; Alzheimer Genetic Analysis Group (2013). TREM2 variants in Alzheimer's disease. N. Engl. J. Med. *368*, 117–127.

Hansen, K.D., Irizarry, R.A., and Wu, Z. (2012). Removing technical variability in RNA-seq data using conditional quantile normalization. Biostatistics *13*, 204–216.

Hebert, L.E., Weuve, J., Scherr, P.A., and Evans, D.A. (2013). Alzheimer disease in the United States (2010-2050) estimated using the 2010 census. Neurology *80*, 1778–1783.

Heit, C., Jackson, B.C., McAndrews, M., Wright, M.W., Thompson, D.C., Silverman, G.A., Nebert, D.W., and Vasiliou, V. (2013). Update of the human and mouse SERPIN gene superfamily. Hum. Genomics *7*, 22.

Holtzman, D.M., Herz, J., and Bu, G. (2012). Apolipoprotein E and apolipoprotein E receptors: normal biology and roles in Alzheimer disease. Cold Spring Harb. Perspect. Med. *2*, a006312.

CellPress

Horvath, A.J., Irving, J.A., Rossjohn, J., Law, R.H., Bottomley, S.P., Quinsey, N.S., Pike, R.N., Coughlin, P.B., and Whisstock, J.C. (2005). The murine orthologue of human antichymotrypsin: a structural paradigm for clade A3 serpins. J. Biol. Chem. *280*, 43168–43178.

Hu, Z., Chang, Y.C., Wang, Y., Huang, C.L., Liu, Y., Tian, F., Granger, B., and Delisi, C. (2013). VisANT 4.0: Integrative network platform to connect genes, drugs, diseases and therapies. Nucleic Acids Res. *41*, W225–W231.

Hu, J., Liu, C.C., Chen, X.F., Zhang, Y.W., Xu, H., and Bu, G. (2015). Opposing effects of viral mediated brain expression of apolipoprotein E2 (apoE2) and apoE4 on apoE lipidation and Aβ metabolism in apoE4-targeted replacement mice. Mol. Neurodegener. *10*, 6.

Irving, J.A., Pike, R.N., Lesk, A.M., and Whisstock, J.C. (2000). Phylogeny of the serpin superfamily: implications of patterns of amino acid conservation for structure and function. Genome Res. *10*, 1845–1864.

Jonsson, T., Stefansson, H., Steinberg, S., Jonsdottir, I., Jonsson, P.V., Snaedal, J., Bjornsson, S., Huttenlocher, J., Levey, A.I., Lah, J.J., et al. (2013). Variant of TREM2 associated with the risk of Alzheimer's disease. N. Engl. J. Med. *368*, 107–116.

Kalari, K.R., Nair, A.A., Bhavsar, J.D., O'Brien, D.R., Davila, J.I., Bockol, M.A., Nie, J., Tang, X., Baheti, S., Doughty, J.B., et al. (2014). MAP-RSeq: Mayo Analysis Pipeline for RNA sequencing. BMC Bioinformatics *15*, 224.

Kanekiyo, T., Xu, H., and Bu, G. (2014). ApoE and Aβ in Alzheimer's disease: accidental encounters or partners? Neuron *81*, 740–754.

Kang, S.S., Ebbert, M.T.W., Baker, K.E., Cook, C., Wang, X., Sens, J.P., Kocher, J.P., Petrucelli, L., and Fryer, J.D. (2018). Microglial translational profiling reveals a convergent APOE pathway from aging, amyloid, and tau. J. Exp. Med. *215*, 2235–2245.

Karjalainen, J.P., Mononen, N., Hutri-Kähönen, N., Lehtimäki, M., Juonala, M., Ala-Korpela, M., Kähönen, M., Raitakari, O., and Lehtimäki, T. (2019). The effect of apolipoprotein E polymorphism on serum metabolome - a population-based 10-year follow-up study. Sci. Rep. *9*, 458.

Keren-Shaul, H., Spinrad, A., Weiner, A., Matcovitch-Natan, O., Dvir-Szternfeld, R., Ulland, T.K., David, E., Baruch, K., Lara-Astaiso, D., Toth, B., et al. (2017). A Unique Microglia Type Associated with Restricting Development of Alzheimer's Disease. Cell *169*, 1276–1290.

Kim, D., Pertea, G., Trapnell, C., Pimentel, H., Kelley, R., and Salzberg, S.L. (2013). TopHat2: accurate alignment of transcriptomes in the presence of insertions, deletions and gene fusions. Genome Biol. *14*, R36.

Kowal, R.C., Herz, J., Weisgraber, K.H., Mahley, R.W., Brown, M.S., and Goldstein, J.L. (1990). Opposing effects of apolipoproteins E and C on lipoprotein binding to low density lipoprotein receptor-related protein. J. Biol. Chem. *265*, 10771–10779.

Krämer, A., Green, J., Pollard, J., Jr., and Tugendreich, S. (2014). Causal analysis approaches in Ingenuity Pathway Analysis. Bioinformatics *30*, 523–530.

Lahoz, C., Schaefer, E.J., Cupples, L.A., Wilson, P.W., Levy, D., Osgood, D., Parpos, S., Pedro-Botet, J., Daly, J.A., and Ordovas, J.M. (2001). Apolipoprotein E genotype and cardiovascular disease in the Framingham Heart Study. Atherosclerosis *154*, 529–537.

Langfelder, P., and Horvath, S. (2008). WGCNA: an R package for weighted correlation network analysis. BMC Bioinformatics *9*, 559.

Langmead, B., Trapnell, C., Pop, M., and Salzberg, S.L. (2009). Ultrafast and memory-efficient alignment of short DNA sequences to the human genome. Genome Biol. *10*, R25.

Law, R.H., Zhang, Q., McGowan, S., Buckle, A.M., Silverman, G.A., Wong, W., Rosado, C.J., Langendorf, C.G., Pike, R.N., Bird, P.I., and Whisstock, J.C. (2006). An overview of the serpin superfamily. Genome Biol. *7*, 216.

Liao, Y., Smyth, G.K., and Shi, W. (2014). featureCounts: an efficient general purpose program for assigning sequence reads to genomic features. Bioinformatics *30*, 923–930.

Liu, C.C., Zhao, N., Fu, Y., Wang, N., Linares, C., Tsai, C.W., and Bu, G. (2017). ApoE4 Accelerates Early Seeding of Amyloid Pathology. Neuron *96*, 1024–1032.

Loy, C.T., Schofield, P.R., Turner, A.M., and Kwok, J.B. (2014). Genetics of dementia. Lancet *383*, 828–840.

Mahley, R.W. (2016). Central Nervous System Lipoproteins: ApoE and Regulation of Cholesterol Metabolism. Arterioscler. Thromb. Vasc. Biol. *36*, 1305–1315.

Maly, D.J., and Papa, F.R. (2014). Druggable sensors of the unfolded protein response. Nat. Chem. Biol. *10*, 892–901.

Mapstone, M., Cheema, A.K., Fiandaca, M.S., Zhong, X., Mhyre, T.R., MacArthur, L.H., Hall, W.J., Fisher, S.G., Peterson, D.R., Haley, J.M., et al. (2014). Plasma phospholipids identify antecedent memory impairment in older adults. Nat. Med. *20*, 415–418.

Mayeux, R., Saunders, A.M., Shea, S., Mirra, S., Evans, D., Roses, A.D., Hyman, B.T., Crain, B., Tang, M.X., and Phelps, C.H.; Alzheimer's Disease Centers Consortium on Apolipoprotein E and Alzheimer's Disease (1998). Utility of the apolipoprotein E genotype in the diagnosis of Alzheimer's disease. N. Engl. J. Med. *338*, 506–511.

Mazure, C.M., and Swendsen, J. (2016). Sex differences in Alzheimer's disease and other dementias. Lancet Neurol. *15*, 451–452.

McGeer, P.L., McGeer, E., Rogers, J., and Sibley, J. (1990). Anti-inflammatory drugs and Alzheimer disease. Lancet *335*, 1037.

Michaelson, D.M. (2014). APOE ε4: the most prevalent yet understudied risk factor for Alzheimer's disease. Alzheimers Dement. *10*, 861–868.

Neu, S.C., Pa, J., Kukull, W., Beekly, D., Kuzma, A., Gangadharan, P., Wang, L.S., Romero, K., Arneric, S.P., Redolfi, A., et al. (2017). Apolipoprotein E Genotype and Sex Risk Factors for Alzheimer Disease: A Meta-analysis. JAMA Neurol. *74*, 1178–1189.

Padmanabhan, J., Levy, M., Dickson, D.W., and Potter, H. (2006). Alpha1-antichymotrypsin, an inflammatory protein overexpressed in Alzheimer's disease brain, induces tau phosphorylation in neurons. Brain *129*, 3020–3034.

Pasternack, J.M., Abraham, C.R., Van Dyke, B.J., Potter, H., and Younkin, S.G. (1989). Astrocytes in Alzheimer's disease gray matter express alpha 1-antichymotrypsin mRNA. Am. J. Pathol. *135*, 827–834.

Pathan, M., Fonseka, P., Chitti, S.V., Kang, T., Sanwlani, R., Van Deun, J., Hendrix, A., and Mathivanan, S. (2019). Vesiclepedia 2019: a compendium of RNA, proteins, lipids and metabolites in extracellular vesicles. Nucleic Acids Res. *47* (D1), D516–D519.

Payami, H., Montee, K.R., Kaye, J.A., Bird, T.D., Yu, C.E., Wijsman, E.M., and Schellenberg, G.D. (1994). Alzheimer's disease, apolipoprotein E4, and gender. JAMA *271*, 1316–1317.

Perez-Nievas, B.G., and Serrano-Pozo, A. (2018). Deciphering the Astrocyte Reaction in Alzheimer's Disease. Front. Aging Neurosci. *10*, 114.

Phillips, M.C. (2014). Apolipoprotein E isoforms and lipoprotein metabolism. IUBMB Life *66*, 616–623.

Ping, L., Duong, D.M., Yin, L., Gearing, M., Lah, J.J., Levey, A.I., and Seyfried, N.T. (2018). Global quantitative analysis of the human brain proteome in Alzheimer's and Parkinson's Disease. Sci. Data *5*, 180036.

Pitale, P.M., Gorbatyuk, O., and Gorbatyuk, M. (2017). Neurodegeneration: Keeping ATF4 on a Tight Leash. Front. Cell. Neurosci. *11*, 410.

Poliani, P.L., Wang, Y., Fontana, E., Robinette, M.L., Yamanishi, Y., Gilfillan, S., and Colonna, M. (2015). TREM2 sustains microglial expansion during aging and response to demyelination. J. Clin. Invest. *125*, 2161–2170.

Rangaraju, S., Dammer, E.B., Raza, S.A., Rathakrishnan, P., Xiao, H., Gao, T., Duong, D.M., Pennington, M.W., Lah, J.J., Seyfried, N.T., and Levey, A.I. (2018). Identification and therapeutic modulation of a pro-inflammatory subset of disease-associated-microglia in Alzheimer's disease. Mol. Neurodegener. *13*, 24.

Rasmussen, K.L., Tybjaerg-Hansen, A., Nordestgaard, B.G., and Frikke-Schmidt, R. (2015). Plasma levels of apolipoprotein E and risk of dementia in the general population. Ann. Neurol. *77*, 301–311.

Sala Frigerio, C., Wolfs, L., Fattorelli, N., Thrupp, N., Voytyuk, I., Schmidt, I., Mancuso, R., Chen, W.T., Woodbury, M.E., Srivastava, G., et al. (2019). The

Major Risk Factors for Alzheimer's Disease: Age, Sex, and Genes Modulate the Microglia Response to Abeta Plaques. Cell Rep. *27*, 1293–1306.

Scheper, W., and Hoozemans, J.J. (2015). The unfolded protein response in neurodegenerative diseases: a neuropathological perspective. Acta Neuropathol. *130*, 315–331.

Schneider, W.J., Kovanen, P.T., Brown, M.S., Goldstein, J.L., Utermann, G., Weber, W., Havel, R.J., Kotite, L., Kane, J.P., Innerarity, T.L., and Mahley, R.W. (1981). Familial dysbetalipoproteinemia. Abnormal binding of mutant apoprotein E to low density lipoprotein receptors of human fibroblasts and membranes from liver and adrenal of rats, rabbits, and cows. J. Clin. Invest. *68*, 1075–1085.

Shi, Y., Yamada, K., Liddelow, S.A., Smith, S.T., Zhao, L., Luo, W., Tsai, R.M., Spina, S., Grinberg, L.T., Rojas, J.C., et al.; Alzheimer's Disease Neuroimaging Initiative (2017). ApoE4 markedly exacerbates tau-mediated neurodegeneration in a mouse model of tauopathy. Nature *549*, 523–527.

Shinohara, M., Kanekiyo, T., Yang, L., Linthicum, D., Shinohara, M., Fu, Y., Price, L., Frisch-Daiello, J.L., Han, X., Fryer, J.D., and Bu, G. (2016). APOE2 eases cognitive decline during Aging: Clinical and preclinical evaluations. Ann. Neurol. *79*, 758–774.

Song, W.M., and Colonna, M. (2018). The identity and function of microglia in neurodegeneration. Nat. Immunol. *19*, 1048–1058.

St John-Williams, L., Blach, C., Toledo, J.B., Rotroff, D.M., Kim, S., Klavins, K., Baillie, R., Han, X., Mahmoudiandehkordi, S., Jack, J., et al.; Alzheimer's Disease Neuroimaging Initiative; Alzheimer's Disease Metabolomics Consortium (2017). Targeted metabolomics and medication classification data from participants in the ADNI1 cohort. Sci. Data *4*, 170140.

Sullivan, P.M., Mezdour, H., Aratani, Y., Knouff, C., Najib, J., Reddick, R.L., Quarfordt, S.H., and Maeda, N. (1997). Targeted replacement of the mouse apolipoprotein E gene with the common human APOE3 allele enhances diet-induced hypercholesterolemia and atherosclerosis. J. Biol. Chem. *272*, 17972–17980.

Tachibana, M., Holm, M.L., Liu, C.C., Shinohara, M., Aikawa, T., Oue, H., Yamazaki, Y., Martens, Y.A., Murray, M.E., Sullivan, P.M., et al. (2019). APOE4-mediated amyloid-β pathology depends on its neuronal receptor LRP1. J. Clin. Invest. *129*, 1272–1277.

Uddin, M.S., Stachowiak, A., Mamun, A.A., Tzvetkov, N.T., Takeda, S., Atanasov, A.G., Bergantin, L.B., Abdel-Daim, M.M., and Stankiewicz, A.M. (2018). Autophagy and Alzheimer's Disease: From Molecular Mechanisms to Therapeutic Implications. Front. Aging Neurosci. Published online January 30, 2018. https://doi.org/10.3389/fnagi.2018.00004.

Ulland, T.K., and Colonna, M. (2018). TREM2 - a key player in microglial biology and Alzheimer disease. Nat. Rev. Neurol. *14*, 667–675.

Walker, D.G., and Lue, L.F. (2015). Immune phenotypes of microglia in human neurodegenerative disease: challenges to detecting microglial polarization in human brains. Alzheimers Res. Ther. *7*, 56.

Walter, P., and Ron, D. (2011). The unfolded protein response: from stress pathway to homeostatic regulation. Science *334*, 1081–1086.

Wang, L., Wang, S., and Li, W. (2012). RSeQC: quality control of RNA-seq experiments. Bioinformatics *28*, 2184–2185.

Wilson, P.W., Myers, R.H., Larson, M.G., Ordovas, J.M., Wolf, P.A., and Schaefer, E.J. (1994). Apolipoprotein E alleles, dyslipidemia, and coronary heart disease. The Framingham Offspring Study. JAMA *272*, 1666–1671.

Xia, X., Jiang, Q., McDermott, J., and Han, J.J. (2018). Aging and Alzheimer's disease: Comparison and associations from molecular to system level. Aging Cell *17*, e12802.

Yamazaki, Y., and Kanekiyo, T. (2017). Blood-Brain Barrier Dysfunction and the Pathogenesis of Alzheimer's Disease. Int. J. Mol. Sci. *18*, 18.

Yamazaki, Y., Zhao, N., Caulfield, T.R., Liu, C.C., and Bu, G. (2019). Apolipoprotein E and Alzheimer disease: pathobiology and targeting strategies. Nat. Rev. Neurol. *15*, 501–518.

Zamanian, J.L., Xu, L., Foo, L.C., Nouri, N., Zhou, L., Giffard, R.G., and Barres, B.A. (2012). Genomic analysis of reactive astrogliosis. J. Neurosci. *32*, 6391–6410.

Zhang, B., and Horvath, S. (2005). A general framework for weighted gene co-expression network analysis. Stat. Appl. Genet. Mol. Biol. *4*, Article17.

Zhang, B., Gaiteri, C., Bodea, L.G., Wang, Z., McElwee, J., Podtelezhnikov, A.A., Zhang, C., Xie, T., Tran, L., Dobrin, R., et al. (2013). Integrated systems approach identifies genetic nodes and networks in late-onset Alzheimer's disease. Cell *153*, 707–720.

Zhao, N., Liu, C.C., Van Ingelgom, A.J., Martens, Y.A., Linares, C., Knight, J.A., Painter, M.M., Sullivan, P.M., and Bu, G. (2017a). Apolipoprotein E4 Impairs Neuronal Insulin Signaling by Trapping Insulin Receptor in the Endosomes. Neuron *96*, 115–129.

Zhao, Q.R., Lei, Y.Y., Li, J., Jiang, N., and Shi, J.P. (2017b). Association between apolipoprotein E polymorphisms and premature coronary artery disease: a meta-analysis. Clin. Chem. Lab. Med. *55*, 284–298.

Zhao, N., Liu, C.C., Qiao, W., and Bu, G. (2018a). Apolipoprotein E, Receptors, and Modulation of Alzheimer's Disease. Biol. Psychiatry *83*, 347–357.

Zhao, N., Liu, C.C., Van Ingelgom, A.J., Linares, C., Kurti, A., Knight, J.A., Heckman, M.G., Diehl, N.N., Shinohara, M., Martens, Y.A., et al. (2018b). APOE ε2 is associated with increased tau pathology in primary tauopathy. Nat. Commun. *9*, 4388.

Zhao, N., Attrebi, O.N., Ren, Y., Qiao, W., Sonustun, B., Martens, Y.A., Meneses, A.D., Li, F., Shue, F., Zheng, J., et al. (2020). APOE4 exacerbates α-synuclein pathology and related toxicity independent of amyloid. Sci. Transl. Med. *12*. Published online February 5, 2020. https://doi.org/10.1126/scitranslmed.aay1809.

Zhu, Y., Nwabuisi-Heath, E., Dumanis, S.B., Tai, L.M., Yu, C., Rebeck, G.W., and LaDu, M.J. (2012). APOE genotype alters glial activation and loss of synaptic markers in mice. Glia *60*, 559–569.

STAR★METHODS

KEY RESOURCES TABLE

REAGENT or RESOURCE	SOURCE	IDENTIFIER
Antibodies		
Serpina3n	R&D systems	Cat# AF4709; RRID:AB_2270116
α-tubulin	Sigma	Cat# T9026; RRID:AB_477593
β-actin	Cell Signaling Technology	Cat# 4967L; RRID:AB_330288
CD68	Abcam	Cat# ab125212; RRID:AB_10975465
IBA1	WAKO	Cat# 019-19741; RRID:AB_839504
Chemicals		
Trizol	Trizol	Trizol
RNeasy Mini Kit	RNeasy Mini Kit	RNeasy Mini Kit
Critical Commercial Assays		
AbsoluteIDQ p180 kit	Biocrates	https://biocrates.com/absoluteidq-p180-kit/
cBot and HiSeq 3000/4000 PE Cluster Kit	Illumina	RRID: SCR_010233
TruSeq RNA Sample Prep Kit v2	Illumina	RRID: SCR_010233
HiSeq 3000/4000 sequencing kit	Illumina	RRID: SCR_010233
HCS v3.3.52 collection software	Illumina	RRID: SCR_010233
Mouse Serpina3 ELISA kit	Cusabio	Cat# CSB-E13727m
RNAscope® Multiplex Fluorescent Reagent Manual Assay Kit v2	ACD	Cat #323100
Deposited Data		
Raw data and analysis for brain transcriptomics	This paper	https://doi.org/10.7303/syn20808171
Raw data and analysis for serum metabolomics	This paper	https://doi.org/10.7303/syn20808172
Mayo Clinic human brain RNA-seq raw data	(Allen et al., 2016)	https://www.synapse.org/ Synapse ID: syn5550404
ROSMAP human brain RNA-seq raw data	(Bennett et al., 2018)	https://www.synapse.org/ Synapse ID: syn3219045
Human brain proteomics raw data	(Ping et al., 2018)	https://www.synapse.org/ Synapse ID: syn10183278
Mouse reference genome mm10	Genome Reference Consortium	http://useast.ensembl.org/Mus_musculus/Info/Annotation
Experimental Models: Organisms/Strains		
Mouse/apoE2-TR (B6.129P2-$Apoe^{tm1(APOE2)Mae}$ N9)	Taconic Biosciences	RRID: IMSR_TAC:1547
Mouse/apoE3-TR (B6.129P2-$Apoe^{tm2(APOE3)Mae}$ N8)	Taconic Biosciences	RRID: IMSR_TAC:1548
Mouse/apoE4-TR (B6.129P2-$Apoe^{tm3(APOE4)Mae}$ N8)	Taconic Biosciences	RRID: IMSR_TAC:1549
Oligonucleotides		
Mouse Serpina3n	ACD	Cat #430191
DapB	ACD	Cat #310043
Ppib	ACD	Cat #313911
Software and Algorithms		
RTA version 2.7.3	Illumina	RRID: SCR_010233
R version 3.4.2	R Core Team	https://www.R-project.org/

(Continued on next page)

Continued

REAGENT or RESOURCE	SOURCE	IDENTIFIER
MAP-RSeq version 2.1.1	(Kalari et al., 2014)	http://bioinformaticstools.mayo.edu/research/maprseq/
TopHat version 2.1.0	(Kim et al., 2013)	https://ccb.jhu.edu/software/tophat/index.shtml
Bowtie version 1.1.2	(Langmead et al., 2009)	https://sourceforge.net/projects/bowtie-bio/files/bowtie/1.1.2/
RSeQC version 2.6.2	(Wang et al., 2012)	http://rseqc.sourceforge.net/
featureCounts version 1.4.6-p5	(Liao et al., 2014)	http://subread.sourceforge.net
CQN version 1.24.0	(Hansen et al., 2012)	https://bioconductor.org/packages/release/bioc/html/cqn.html
Partek Genomics Suite version 6.6	Partek	https://www.partek.com/
Ingenuity Pathway Analysis version 2019-05-15	QIAGEN	https://digitalinsights.qiagen.com/products/ingenuitypathway-analysis
WGCNA version 1.61	(Langfelder and Horvath, 2008)	https://horvath.genetics.ucla.edu/html/CoexpressionNetwork/Rpackages/WGCNA/
anRichment version 0.82-1	(Langfelder and Horvath, 2008)	https://horvath.genetics.ucla.edu/html/CoexpressionNetwork/GeneAnnotation/index.html
VisANT version 5.51	(Hu et al., 2013)	http://visant.bu.edu/home2.htm
MATLAB	MathWorks	https://www.mathworks.com/products/matlab.html
Prism 7.0	GraphPad Software	https://www.graphpad.com/
Other		
Resource website	This paper	http://www.gbulab.com/searchlinks

LEAD CONTACT AND MATERIALS AVAILABILITY

Further information and requests for resources and reagents should be directed to and will be fulfilled by the Lead Contact, Guojun Bu (bu.guojun@mayo.edu). This study did not generate new unique reagents.

EXPERIMENTAL MODEL AND SUBJECT DETAILS

Mice
ApoE-targeted replacement (apoE-TR) mice in which murine *Apoe* gene locus is replaced with human *APOE2*, *APOE3*, or *APOE4* gene (Sullivan et al., 1997) were obtained from Taconic Biosciences. Animals were housed under controlled temperature and lighting conditions and were given free access to food and water. Male and female apoE-TR mice at 3, 12 and 24 months of age were sacrificed (n = 8 mice/genotype/sex/age group). Mice were anesthetized with isoflurane and blood was collected from the inferior vena cava. After transcardial perfusion with phosphate-buffered saline (PBS, pH 7.4), the brains were collected and divided along the sagittal plane. Cortex from left hemisphere was snap-frozen in liquid nitrogen immediately and further stored at −80°C for RNA extraction and RNA-Seq. Blood was stored at 4°C overnight and then centrifuged at 1000 x g for 10 minutes. The serum was collected and stored at −80°C for metabolomics study. All animal procedures were approved by the Mayo Clinic Institutional Animal Care and Use Committee (IACUC) and were in accordance with the National Institutes of Health Guide for the Care and Use of Laboratory Animals.

Humans
The RNA sequencing data of the ROSMAP (Bennett et al., 2018) and Mayo Clinic post mortem brain samples (Allen et al., 2016; Allen et al., 2018a) were used for gene module preservation analyses. Briefly, 150 AD (cogdx = 4, Braak ≥ 4, CERAD ≤ 2), 78 mild cognitive impairment (MCI; cogdx = 2, Braak ≥ 4) and 85 no cognitive impairment (NCI, control; cogdx = 1, Braak ≤ 3, CERAD ≥ 3) white, non-Hispanic samples from prefrontal cortex of ROSMAP cohort were analyzed. For Mayo Clinic cohorts, the data of temporal cortex from 82 AD and 77 controls, and the cerebellum from 82 AD and 76 controls were analyzed. Additionally, we analyzed the module preservation using the previously published protein expression profiles from dorsolateral prefrontal frontal cortex and anterior cingulate gyrus of 10 AD and 10 controls subjects measured by liquid chromatography-tandem mass spectrometry (Ping et al., 2018).

METHOD DETAILS

Brain tissue RNA extraction, library preparation and sequencing

Total RNA were extracted from the cortex using Trizol reagent (Thermo Fisher Scientific, Waltham, MA) and cleaned using RNeasy spin columns with DNase treatment (QIAGEN, Hilden, Germany) to remove contaminating genomic DNA. The RNA concentrations were determined by NanoDrop™ Spectrophotometers (Thermo Fisher Scientific, Waltham, MA). The RNA integrity numbers (RIN) were measured using an RNA chip on an Agilent Bioanalyzer (Agilent Technologies). The RIN values of all the RNA samples were ≥ 7, thus all samples were approved for library preparation and sequencing. RNA libraries were prepared from 200 ng of total RNA using the TruSeq RNA Sample Prep Kit v2 (Illumina, San Diego, CA) according to the manufacturer's instructions, employing poly-A mRNA enrichment using oligo-dT magnetic beads. The final adaptor-modified cDNA fragments were enriched by 12 cycles of PCR using Illumina TruSeq PCR primers. The concentration and size distribution of the completed libraries were determined using a Fragment Analyzer (AATI, Ankeny, IA) and Qubit fluorometer (Invitrogen, Carlsbad, CA). Libraries were randomized for sequencing lanes and flow cells, and were sequenced following Illumina's standard protocol using the Illumina cBot and HiSeq 3000/4000 PE Cluster Kit, yielding 40 to 75 million fragment reads per sample. Each fragment was sequenced as 50 × 2 paired end reads on an Illumina HiSeq 4000 using HiSeq 3000/4000 sequencing kit and HCS v3.3.52 collection software. Base-calling was performed using Illumina's RTA version 2.7.3.

Serum metabolites detection

Serum samples were analyzed using the AbsoluteIDQ p180 kit (Biocrates Life Sciences AG, Innsbruck, Austria) according to the user manual. Briefly, after the addition of 10 μl of the supplied internal standard solution to each well on filterspot of the 96-well extraction plates, 10 μl of each serum sample, quality control (QC) samples, blank, zero sample, or calibration standard were added to the appropriate wells. All the serum samples were randomly distributed in different plates during detection. The plates were then dried under a gentle stream of nitrogen. The samples were derivatized with phenyl isothiocyanate (PITC) for the amino acids and biogenic amines, and dried again. Sample extract elution was performed with 5 mM ammonium acetate in methanol. Sample extracts were diluted with either 40% methanol in water for the UPLC-MS/MS analysis (15:1) or kit running solvent (Biocrates Life Sciences AG) for flow injection analysis (FIA)-MS/MS (20:1).

Mouse tissue preparation for validation experiments

Mice were deeply anesthetized with isoflurane prior to transcardial perfusion with saline. Brains was removed and bisected along the midline. One half of each brain was drop-fixed in 10% neutral buffered formalin (Fisher Scientific) overnight at 4°C for *in situ* hybridization and histology, and the other half was snap-frozen in liquid nitrogen and stored at −80°C. Livers were collected as well. For biochemical analysis, the brain and liver tissues were homogenized and lysed in RIPA (Fisher Scientific) buffer, supplemented by protease inhibitor (cOmplete) and phosphatase inhibitor (PhosSTOP) and ultracentrifuged at 50,000 g for 30 min at 4°C. The supernatant was collected as RIPA soluble fraction and stored in −80°C.

Histology and immunohistochemistry

The brain samples fixed in 10% formalin were embedded in paraffin wax, sectioned in a coronal plane at 5 μm thickness and mounted on glass slides. Sections were collected from the same brain region for all animals, and brain regions were confirmed under the microscope by comparing sections to images on the Allen Mouse Brain Atlas site. The tissue sections were de-paraffinized in xylene and rehydrated in a graded series of alcohols. Antigen retrieval was performed by steaming in distilled water for 30 min, and endogenous peroxidase activity was blocked by incubation in 0.03% hydrogen peroxide. Sections were then immunostained using the DAKO Autostainer (DAKO) and the DAKO EnVision+HRP system. The stained slides were dehydrated, coverslipped and scanned with the Aperio Slide Scanner (Aperio). The following primary antibodies were used: anti-CD68 (Cat# ab125212, Abcam, 1:2500) and anti-IBA1 (Cat# 019-19741, Wako, 1:2500) antibodies. A technician blinded to sample groups performed immunohistochemical staining. Data collection and quantification of immunoreactivity were performed blindly by another technician.

In situ hybridization

In situ hybridization was performed on freshly cut Formalin-Fixed Paraffin-Embedded 5μm sections using RNAscope® Multiplex Fluorescent Reagent Manual Assay Kit v2 (Cat #323100, ACD) according to the manufacturer's protocol with ACD probes for mouse *Serpina3n* (Cat #430191; target NM_009252.2, 745-2005bp), *DapB* (negative control Cat #310043; target EF191515, 414-862bp), and *Ppib* (positive control Cat #313911; target NM_011149.2, 98-856bp). The probes were detected using AKOYA Biosciences fluorophores Opal 620, diluted 1:750 in TSA Buffer (ACD). The slides were counterstained with DAPI (ACD) for 2 min at RT before mounting.

Western blotting

Equal amounts of protein from RIPA fraction of homogenized tissue lysates were resolved by SDS-PAGE and transferred to PVDF membranes. After the membranes were blocked, proteins of interest were detected with a primary antibody. The membranes were then probed with an HRP-conjugated secondary antibody and visualized using the Odyssey infrared imaging system (LI-COR).

The following primary antibodies were used: anti-Serpin3n (Cat# AF4709, R&D systems, 1:1000), anti-α-tubulin (Cat# T9026, Sigma, 1:5000), and anti-β-actin (Cat# 4967L, Cell Signaling Technology, 1:2000) antibodies.

Serpina3 ELISA
The Serpina3 level in mouse serum was measured using a commercial ELISA kit (Cat# CSB-E13727m, Cusabio) according to the instructions provided by the manufacturer. Briefly, the serum samples were diluted 500 folds with Sample Diluent buffer and 100 μL of samples were added into the antibody-coated plate for 2 hours incubation at 37°C. 100 μL of Biotin-conjugated detection antibodies were then added into the plate and incubated for 1 hour at 37°C. The plate was washed and incubated with 100 μL HRP-avidin for 1 hour at 37°C. After washing, 90 μL TMB were added into the plate with 20 minutes incubation at 37°C with protection from light. 50 μL of the Stop Solution were applied before colorimetric absorbance measurements were taken at 450 nm using a Synergy HT plate reader (BioTek).

qPCR analysis
Reverse transcription of RNA was performed using iScript Reverse Transcription Supermix (Biorad). cDNA was added to a reaction mix (10 μl final volume) containing gene-specific primers and SYBR green supermix (Biorad). All samples were run in duplicates and were analyzed with QuantStudio^{TM} 7 Flex Real-Time PCR System (ThermoFisher Scientific). The relative gene expression was normalized to *Gapdh* controls and assessed using the $2^{-\Delta\Delta CT}$ method. Primer sequences and information are as follows (5′–3′): Gapdh: AGGTCGGTGTGAACGGATTTG (forward) and TGTAGACCATGTAGTTGAGGTCA (reverse); *Serpina3n*: Mm.PT.58.6333775 (Integrated Device Technology, IDT, CA); *Wdfy1*: Mm.PT.58.13459241 (IDT); *Alkbh6*: Mm.PT.58.7880283 (IDT); *C4b*: Mm.PT.58.42828296.g (IDT); *Pcdhb9*: Mm.PT.58.14060200.g (IDT); *Plekhb1*: Mm.PT.58.10308025 (IDT).

QUANTIFICATION AND STATISTICAL ANALYSIS

RNA and metabolites quantification, quality control and normalization
RNA sequencing reads were processed using the Mayo Clinic RNA sequencing analytic pipeline, MAP-RSeq Version 2.1.1 (Kalari et al., 2014). Briefly, reads were aligned to the mouse reference genome mm10 using TopHat version 2.1.0 (Kim et al., 2013) and Bowtie version 1.1.2 (Langmead et al., 2009). Quality control (QC) was performed using RSeQC version 2.6.2 (Wang et al., 2012). Gene counts were generated using featureCounts version 1.4.6-p5 (Liao et al., 2014). One 12 months *APOE2* male sample failed the pipeline and was excluded from further analysis. For the remaining 143 sample, conditional quantile normalization (CQN) was applied to raw gene counts to remove unwanted sources of variability caused by GC-content, gene length, sample-specific systematic biases and global distortions that affect the overall distribution of gene counts (Hansen et al., 2012). Based on the bimodal distribution of the CQN-normalized and log$_2$-transformed reads per kb per million (RPKM) gene expression values, genes with log2 RPKM of −1 or more in at least one sample were considered expressed above detection threshold. Using this selection threshold, 19,120 genes were included in the downstream analyses. Principal component analysis (PCA) identified two sample outliers: a 3 month-old *APOE4* male, and a 12 month-old *APOE4* female, both were excluded from downstream analyses.

Metabolites from 144 serum samples were analyzed using four sets of QC as described in (St John-Williams et al., 2017). First, low/mid/high level QC samples provided by Biocrates Life Sciences AG were prepared and analyzed on each plate as recommended by the manufacturer. These QC samples were used for technical validation of each kit plate. Briefly, metabolites with > 40% of measurements below the lower limit of detection (LOD) were excluded from the analysis. To adjust for batch effects, a correction factor for each metabolite in a specific plate was obtained by dividing the metabolite's QC global average by the QC average within the plate. Using each metabolite's LOD/2 value followed by log2 transformation, we imputed the < LOD values.

Differential gene expression, hierarchical clustering and pathway analysis
Differential gene expression analyses were performed by Partek Genomics Suite (Partek Inc., St. Louis, MO) using CQN-normalized log2RPKM values. Gene expressions between different *APOE* genotypes, ages and sexes were compared using Analyses of Variance models (ANOVA) while adjusting for sequencing depth per sample, which significantly affected the variation in the gene expression values (mean F ratio > 1.5). The Bonferroni correction was applied to adjust for multiple testing. Differentially expressed genes (DEG) were defined by thresholds of Bonferroni-adjusted p value < 0.05 and |fold change| (FC) ≥ 1.2. Hierarchical clustering was performed in MATLAB using the *Clustergram* function based on standardized Euclidean distance metric. Volcano plots were generated in MATLAB using –log10 (p value) as y axis and ± log2 (|FC|) as x axis. Pathway analyses of differentially expressed genes were performed using Ingenuity Pathway Analysis (QIAGEN Inc., https://digitalinsights.qiagen.com/products/ingenuity-pathway-analysis) (Krämer et al., 2014).

Weighted gene co-expression network analysis of the mouse transcriptomes
Weighted gene co-expression network analysis (WGCNA) was performed using residual expression values calculated from adjusting for sequence coverage. Based on the relationship between power and scale independence, the power of 8 was chosen to build scale-free topology using signed hybrid network. We set the minimum modules size as 30, and merged modules whose correlation coefficients were greater than 0.6 (mergeCutHeight = 0.4). Each module was summarized by the first principal component of the

scaled module expression profiles, termed module eigengene (ME). For each module, the module membership (MM) was defined as the correlation between gene expression values and ME. Intramodular hub genes are genes with the highest connectivity to other genes within a given module, and were selected based on the p values of MM. To assess the correlation of modules to *APOE* genotype, age and sex, we defined the *APOE2* genotype as 0, *APOE3* as 1, and *APOE4* as 2; 3 months of age as 3, 12 months as 12, and 24 months as 24; male as 0 and female as 1. Modules were annotated using R package anRichment. MEs of selected modules were compared between *APOE* genotypes, ages and sexes using boxplots showing maximum and minimum values after Tukey's test. Gene-gene connections among top hub genes were visualized using VisANT version 5.51 (Hu et al., 2013).

Module preservation analysis in human RNA samples

The preservation of the mouse modules were tested in the RNA sequencing data of the ROSMAP prefrontal cortex and Mayo Clinic temporal cortex and cerebellum human post mortem brain samples. With the prefrontal cortex data from ROSMAP, we performed CQN normalization on the raw genes counts of these samples. Based on the bimodal distribution of the CQN-normalized and log_2-transformed RPKM gene expression values, we removed genes whose average expressions in AD, MCI and control were all < 0, leaving 15,439 expressed genes. With the available temporal cortex samples from Mayo Clinic cohort, we performed CQN normalization on the raw genes counts of these samples, and removed genes whose average expressions in AD and control were both < 1, leaving 17,176 expressed genes. We calculated residual expression values of these genes from adjusting for the effects of RIN, which significantly contributed to the variation of the gene expression values (mean F ratio > 1.5). For the available cerebellum samples from Mayo Clinic cohort, after CQN normalization of the raw gene counts, we removed genes whose average expressions in AD and controls were both < 1, leaving 21,459 expressed genes. We calculated residual expression values of these genes from adjusting for the effects of RIN (mean F ratio > 1.5). The human genes were matched to the mouse gene names in order to perform module preservation analysis. Separate module preservation analyses were performed for the three datasets using WGCNA. In all analyses, module definitions from the mouse network were used as reference to calculate the z-summary statistics for each module. Z summary score > 2 suggests moderate preservation, and Z summary score > 10 suggests strong preservation. The MEs of selected modules were compared between disease groups using Mann-Whitney U tests.

Module validation in human proteomics samples

We downloaded the previously published protein expression profiles from human dorsolateral prefrontal frontal cortex and anterior cingulate gyrus and calculated residual expression values of these samples from adjusting for the effects of batch and race, both significantly contributing to the variation of the protein expression values (mean F ratio > 1.5). To validate the pink and blue mouse modules in the human proteomics datasets, we matched the protein names to the module gene names, and calculated MEs of the matched proteins using WGCNA. The MEs of the pink and blue modules were compared between AD and control samples using Mann-Whitney *U* tests.

Differential metabolite expression analysis

Differential metabolite expression analyses were performed using Partek Genomics Suite (Partek Inc., St. Louis, MO). Metabolite expressions between different *APOE* genotypes, ages, and sexes were compared using ANOVA. The Bonferroni correction was applied to adjust for multiple testing. Differentially expressed metabolites (DEM) were defined by thresholds of Bonferroni-adjusted p value < 0.05 and |FC| $\geq$ 1.2. Hierarchical clustering was performed in MATLAB using the *Clustergram* function based on standardized Euclidean distance metric.

Metabolite co-expression network analysis

WGCNA was performed using the metabolite expression values. Based on the relationship between power and scale independence, the power of 16 was chosen to build scale-free topology using unsigned network. We set the minimum modules size as 5, and merged modules whose correlation coefficients were greater than 0.85 (mergeCutHeight = 0.15). Each module was summarized by ME. Hub metabolites were selected based on the p values of MM. To assess the correlation of modules to *APOE* genotype, age and sex, we defined the *APOE2* genotype as 0, *APOE3* as 1, and *APOE4* as 2; 3 months of age as 3, 12 months as 12, and 24 months as 24; male as 0 and female as 1. MEs of selected modules were compared between *APOE* genotypes, ages, and sexes using boxplots showing maximum and minimum values after Tukey's test. The connections among top hub metabolites were visualized using VisANT version 5.51 (Hu et al., 2013).

Statistical analyses for validation experiments

All data were reported as mean values ± SEM unless elsewise indicated. In order to ensure that results were valid in the presence of non-normal distributions, or differing variances between groups, nonparametric Mann-Whitney tests and Kruskal-Wallis tests with Dunn's multiple comparison tests were used to compare outcomes. With sample size < 8, one-way ANOVA was used to compare outcomes among groups. All statistical tests were two-sided. The statistical tests used for each analysis, the numerosity of the experiments, and the significance levels were reported in the caption of each figure.

CellPress

DATA AND CODE AVAILABILITY

Mouse transcriptomic and metabolomics data are available via the AD Knowledge Portal (https://adknowledgeportal.org). The AD Knowledge Portal is a platform for accessing data, analyses, and tools generated by the Accelerating Medicines Partnership (AMP-AD) Target Discovery Program and other National Institute on Aging (NIA)-supported programs to enable open-science practices and accelerate translational learning. Data is available for general research use according to the following requirements for data access and data attribution (https://adknowledgeportal.synapse.org/#/DataAccess/Instructions).

See the following links for data access:

Transcriptomics: https://doi.org/10.7303/syn20808171

Metabolomics: https://doi.org/10.7303/syn20808172

For additional information, see the APOE-TR study (https://adknowledgeportal.synapse.org/Explore/Studies?Study=syn8391648)

ADDITIONAL RESOURCES

Our mouse transcriptomic and metabolomics datasets are also available and can be visualized in the website https://www.gbulab.com/searchlinks.